

Review

# Impact of Titanium Dioxide (TiO<sub>2</sub>) Modification on Its Application to Pollution Treatment—A Review

Ruixiang Li, Tian Li \* and Qixing Zhou \* 

MOE Key Laboratory of Pollution Processes and Environmental Criteria/Tianjin Key Laboratory of Environmental Remediation and Pollution Control/College of Environmental Science and Engineering, Nankai University, No. 38 Tongyan Road, Jinnan District, Tianjin 300350, China; ruixiang1998@163.com

\* Correspondence: tianli1@nankai.edu.cn (T.L.); zhouq1x@163.com (Q.Z.); Tel.: +(86)22-5889-0402 (T.L. & Q.Z.); Fax: +(86)22-2350-1117 (T.L. & Q.Z.)

Received: 12 July 2020; Accepted: 17 July 2020; Published: 20 July 2020



**Abstract:** A high-efficiency method to deal with pollutants must be found because environmental problems are becoming more serious. Photocatalytic oxidation technology as the environmentally-friendly treatment method can completely oxidate organic pollutants into pollution-free small-molecule inorganic substances without causing secondary pollution. As a widely used photocatalyst, titanium dioxide (TiO<sub>2</sub>) can greatly improve the degradation efficiency of pollutants, but several problems are noted in its practical application. TiO<sub>2</sub> modified by different materials has received extensive attention in the field of photocatalysis because of its excellent physical and chemical properties compared with pure TiO<sub>2</sub>. In this review, we discuss the use of different materials for TiO<sub>2</sub> modification, highlighting recent developments in the synthesis and application of TiO<sub>2</sub> composites using different materials. Materials discussed in the article can be divided into nonmetallic and metallic. Mechanisms of how to improve catalytic performance of TiO<sub>2</sub> after modification are discussed, and the future development of modified TiO<sub>2</sub> is prospected.

**Keywords:** TiO<sub>2</sub>; modification; materials; application

## 1. Introduction

In recent years, photocatalytic technology has attracted extensive attention because it is environmentally friendly, low-cost, and has efficient characteristics. In 1972, Fujishima et al. [1] reported that TiO<sub>2</sub> was used as a photoelectrocatalyst to split water into hydrogen. Since then, increasing research has focused on TiO<sub>2</sub>. In 1976, Carey et al. [2] used photocatalytic technology to treat polychlorinated biphenyls, an organic pollution that is difficult to degrade, and experimental results found that the dechlorination rate of polychlorinated biphenyls was close to 100%. In 1977, Frank et al. [3] found that TiO<sub>2</sub> could effectively degrade cyanide (CN<sup>-</sup>), which was the beginning of photocatalytic technology applied to pollution control. The degradation of photocatalytic technology can be summarized into four stages: photoexcitation, carrier capture, formation of radicals, and oxidation reaction. Compared with traditional catalytic technologies, photocatalytic technology has many advantages. First, reaction conditions such as sunlight, room temperature, and normal atmospheric pressure are common and easy to obtain. Second, the degradation processes and products of catalytic decomposition are pollution free, which are in line with the requirements of low-carbon environmental protection. Third, the characteristics of non-toxic, stable, low cost, and recyclable further promote development [4]. The core of photocatalytic technology is the photocatalyst, and many materials can act as a photocatalyst [5]. Table 1 shows the published data of different photocatalysts, including TiO<sub>2</sub> [6–8], SrTiO<sub>3</sub> [9–11], ZnO [12–14], WO<sub>3</sub> [15–17], ZrO<sub>2</sub> [18–20], and g-C<sub>3</sub>N<sub>4</sub> [21–23], and their performance. Among these photocatalysts, TiO<sub>2</sub> occupies an important position due to its stable

physical and chemical properties, strong oxidation capacity, high photocatalytic activity, and excellent biocompatibility [24–26].

The TiO<sub>2</sub> can be synthesized by many methods and mainly include precipitation method, solvothermal method, sol-gel method, microemulsion method, spray pyrolysis method and electrochemical synthesis method. Zhang et al. [27] prepared the TiO<sub>2</sub>/BC catalyst material by the sol-gel method and the degradation rates of reactive brilliant blue KN-R in the dyeing wastewater can reach 97%. However, there are still has some problems of pure TiO<sub>2</sub> in application. The rapid recombination of photo-generated electron-hole pairs is the biggest obstacle that affect the practical application of TiO<sub>2</sub> [28], because recombination of photogenerated charge carriers can reduce the overall quantum efficiency [29]. The poor photosensitivity of TiO<sub>2</sub> under visible/solar irradiation is also a problem [30,31]. Generally, the conventional TiO<sub>2</sub> has broad intrinsic band gaps wide band gap (3.2 eV for anatase and 3.0 eV for rutile) which makes the TiO<sub>2</sub> only absorb UV radiation (wavelength < 400 nm), which accounts for only ~5% of the sunlight [32,33]. What is more, nano-TiO<sub>2</sub> is easy to agglomerate, which extremely limits the application. Therefore, in order to solve these problems and improve the catalytic activity of TiO<sub>2</sub> photocatalysts, composites have become mainstream. In addition to the improvement of photocatalysis, composites can yield other benefits. For example, composites can tune the surface properties, i.e., ability to adsorb pollutants. Composites are also beneficial toward the stabilization of nanoparticles against phenomena such as sintering or aggregation [34].

**Table 1.** The published data of different photocatalysts and their performance.

Type	Photocatalysts	Light Source	Target Pollutant	Degradation Rate	Ref.
TiO <sub>2</sub>	MoS <sub>2</sub> /MoO <sub>3</sub> /TiO <sub>2</sub>	300 W Xe lamp	rhodamine B	95%	[6]
	Yb, Er, Ce-codoped TiO <sub>2</sub>	Xe lamp	4-chlorophenol	95%	[7]
	TiO <sub>2</sub> @SiO <sub>2</sub> composites	500 W mercury lamp	methyl orange	99%	[8]
SrTiO <sub>3</sub>	La- SrTiO <sub>3</sub>	500 W Xe lamp	Cr <sup>6+</sup>	84%	[9]
	Ag <sub>3</sub> PO <sub>4</sub> /PANI/Cr: SrTiO <sub>3</sub>	300 W Xe lamp	phenol	99%	[10]
	Ag, Cr-SrTiO <sub>3</sub>	500 W Xe lamp	methyl orange	98%	[11]
ZnO	Cu-ZnO	blue light lamp	Orange II	70%	[12]
	ZnO	sunlight	methylene blue	90%	[13]
	Sr-ZnO	black light	methylene blue	99%	[14]
WO <sub>3</sub>	WO <sub>3</sub>	1500 W Xe lamp	N, N-diethyl-meta-toluamide	60%	[15]
	WO <sub>3</sub> @Cu@PDI	300 W Xe lamp	tetracycline hydrochloride	85%	[16]
	NiO-WO <sub>3</sub>	150 W tungsten lamp	eosin yellow	95%	[17]
ZrO <sub>2</sub>	Ce, Er-codoped ZrO <sub>2</sub>	halogen lamp	rhodamine B	92%	[18]
	Co <sub>3</sub> O <sub>4</sub> -ZrO <sub>2</sub>	visible light	cyanide	100%	[19]
	Cu- ZrO <sub>2</sub>	Visible light	methyl orange	98%	[20]
g-C <sub>3</sub> N <sub>4</sub>	Ag-P-codoped g-C <sub>3</sub> N <sub>4</sub>	8 W visible lamps	sulfamethoxazole	99%	[21]
	AgI/LaFeO <sub>3</sub> /g-C <sub>3</sub> N <sub>4</sub>	500 W Xe lamp	norfloxacin	95%	[22]
	CdS/g-C <sub>3</sub> N <sub>4</sub>	500 W Xe lamp	rhodamine B	96%	[23]

The modification of TiO<sub>2</sub> to overcome the problems in the use of pure TiO<sub>2</sub> is one of the widely studied topics in the field of photocatalysis. Modified TiO<sub>2</sub> can improve its photocatalytic activity from different mechanisms, including the reduction of the band gap of TiO<sub>2</sub>-based materials, the decrease of the probability of recombination between electron and hole. In recent years, different aspects are applied to improve the photocatalytic efficiency of TiO<sub>2</sub>. One of the methods is ion-doped TiO<sub>2</sub> or coupled with other semiconductor composites to reduce the forbidden band width of TiO<sub>2</sub> and increase its absorption wavelength [35–37]. Another way is to deposit precious metals or metal oxides on the surface of TiO<sub>2</sub> and add electron capture agents or use photo-catalysis to prevent TiO<sub>2</sub> photo-generated electron-hole pair recombination thus improve the photocatalytic efficiency of TiO<sub>2</sub> [38–40]. In addition, dye photosensitization and providing a suitable carrier for TiO<sub>2</sub> would be the efficient methods to modify TiO<sub>2</sub> [41].

In recent years, many reviews have been conducted on the modification of TiO<sub>2</sub>. Serpone [42] reviewed the different mechanisms of anion- and cation-doping TiO<sub>2</sub>. He reported that TiO<sub>2</sub> photocatalysts doped with either anions or cations have recently been shown to have their absorption edge red-shifted to lower energies (longer wavelengths), thus enhancing photonic efficiencies of photoassisted surface redox reactions, and author argued that the red-shift of the absorption edge is due to the formation of color centers. Devi and Kavitha [43] reviewed the photocatalytic activity of non-metal doped TiO<sub>2</sub> for a wide variety of pollutant degradation under UV/visible light, with special emphasis on nitrogen-doped TiO<sub>2</sub>. They also discussed the mechanisms of photocatalytic reactions according to the charge carrier generation–separation–transfer–recombination dynamics together with pollutant adsorption and their reactions with reactive oxygenated species in liquid or gaseous regime. Asahi et al. [44] reviewed previous studies on nonmetal-doped TiO<sub>2</sub> for visible-light sensitization. Among the enormous number of studies and references on this topic, they focused on N-doped TiO<sub>2</sub>. The present review will concentrate on the application of modified TiO<sub>2</sub> in different media. First, this review summarizes the principles and types of different materials for modifying TiO<sub>2</sub>. Then, it discusses the application and progress of modified TiO<sub>2</sub> in treating different pollutants. Finally, it assesses the critical application challenges and potential future research directions.

## 2. Non-Metallic Materials Modified TiO<sub>2</sub>

### 2.1. Non-Metallic Materials Supported TiO<sub>2</sub>

Loading TiO<sub>2</sub> on the carrier can effectively overcome the problems mentioned above [45]. At present, the non-metallic materials commonly used in loading TiO<sub>2</sub> can be divided into non-metallic porous minerals, glasses, carbon materials, and polymer materials.

The treatment of polluted water by porous mineral composites has aroused attention because of the advantages of high specific surface area, strong adsorption characteristics, and the ability of targeted enrichment of pollutants with the development of non-metallic porous minerals. [46]. As shown in Figure 1, TiO<sub>2</sub> loads into the pores or surfaces of mineral materials and then forms the non-metallic porous minerals/nano-TiO<sub>2</sub> composite system, which can solve the problem of the agglomeration of nano-TiO<sub>2</sub> particles. Pollutants can be adsorbed to the surface of nano-TiO<sub>2</sub> through the ion exchange and increase the contact probability of catalysts with pollutants to improve the degradation rate. Hence, porous mineral/nano-TiO<sub>2</sub> composite systems can improve the photodegradation efficiency of nano-TiO<sub>2</sub>. Liang et al. [47] used montmorillonite as the matrix to prepare a TiO<sub>2</sub>/montmorillonite composite photocatalyst. The results showed that the montmorillonite matrix improved the capacity of optical absorption capacity from 70% to 87% because the visible light absorption ability (390–780 nm) of the composites was enhanced compared with pure TiO<sub>2</sub>. Moreover, the ultraviolet light absorption ability of montmorillonite-supported nano-TiO<sub>2</sub> composites was improved. Therefore, adding montmorillonite carrier enhances the absorbance of visible light and ultraviolet light. Zhu et al. [48] prepared Mn-TiO<sub>2</sub>/sepiolite photocatalytic material using the sol-gel method at different calcining temperatures. They found that the degradation rate of emerald dye could reach 98% when the

calcining temperature was 400 °C because sepiolite and Mn broaden the spectral response range of TiO<sub>2</sub>. Saqib et al. [49] prepared a nano-TiO<sub>2</sub> supported on zeolite using the liquid impregnation method. The experimental results showed that the degradation rate of methylene blue (MB) dye by the loaded material was four times that of pure TiO<sub>2</sub> because zeolite has a UV-visible radiation transparency, which allowed the excitation of light to penetrate into opaque solid powder and reach the substrate molecules present in intraparticles spaces. Zeolite might have substantially enhanced the proximity of organic molecules to the available active sites where the degradation reaction needs to take place.

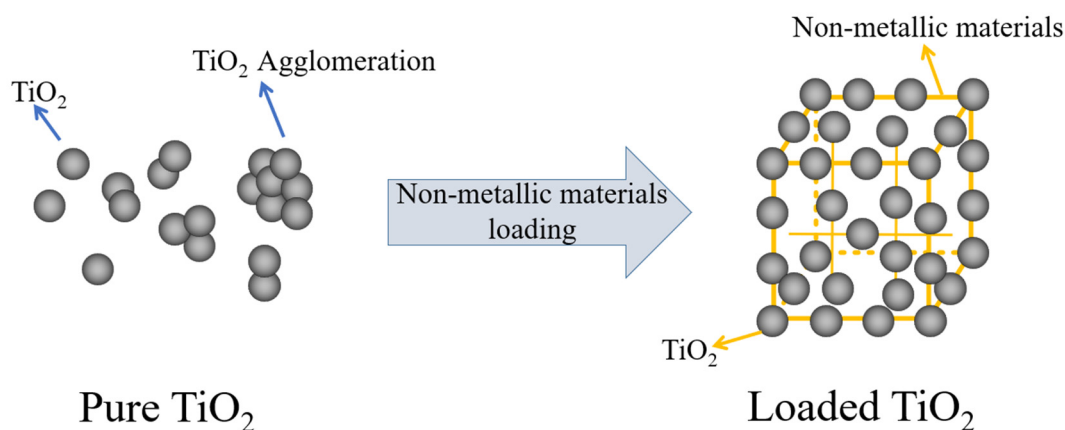


**Figure 1.** The schematic diagram of non-metallic materials loading TiO<sub>2</sub>.

Glass has good light transmission properties and is easy to make into photoreactors with different shapes. Therefore, glass-based carriers have also received widespread attention. The form of glass carrier includes glass sheet, glass tube, glass spring, hollow glass bead, and glass fiber. Malakootian et al. [50] fixed nano-TiO<sub>2</sub> on a glass plate and the removal rate of ciprofloxacin by the composite material reached 93%. Espino-Estévez et al. [51] attached the self-made high-activity TiO<sub>2</sub> to the inner wall of the glass tube reactor by the dipping-lifting method. These results showed that the material had good photocatalytic effect and recycling performance under the ultraviolet light for the degradation of phenol, diclofenac and isoproturon. The degradation rates reached 81% for phenol, 68% for diclofenac and 57% for isoproturon. This was because the decrease of the size of the TiO<sub>2</sub> aggregates. The SEM images showed that coatings prepared after milling the TiO<sub>2</sub> suspension were more homogeneous without surface aggregates, which increased the contact area with pollutants. However, the glass surface is relatively smooth, which makes TiO<sub>2</sub> have poor adhesion on it and causes uneven loading of TiO<sub>2</sub>.

Combining carbon materials with TiO<sub>2</sub> can substantially improve the photocatalytic activity of TiO<sub>2</sub> mainly because C in the carbon material can effectively promote the separation of photogenerated electrons and holes as an electron trap [52]. Carbon materials include carbon fiber (CF), carbon nitride, activated carbon, carbon nanotubes, and graphene. Chu et al. [53] used the microwave hydrothermal method to load nano-TiO<sub>2</sub> on CF. The experimental results showed that TiO<sub>2</sub>/CF has a good photocatalytic activity. The degradation rate of rhodamine B after 1 h of ultraviolet light irradiation reached 95%. When the catalyst was used for 10 cycles, the degradation rate of the dye still reached 88%. They also reported that compared with pure TiO<sub>2</sub> particles, TiO<sub>2</sub>/CF was easily recycled when used as a photocatalyst. Nitric acid oxidation treatment of CF generated polar functional groups, which improved the bonding properties between TiO<sub>2</sub> and CF. Hu et al. [54] prepared 3D flower-like g-C<sub>3</sub>N<sub>4</sub>/TiO<sub>2</sub> composite spherical materials (FCTCMs) using a simple solvothermal method and studied their photocatalytic performance. The results showed that the photocatalytic performance of FCTCMs under visible light was twice that of FTMs (3D flower-like structure of TiO<sub>2</sub> microspheres) because g-C<sub>3</sub>N<sub>4</sub> can broaden the photoresponse range and reduce the recombination rate of photogenerated electron-hole pairs. Cunha et al. [55] prepared TiO<sub>2</sub>/activated carbon composites (TiO<sub>2</sub>/AC), and the

degradation rate of benzodiazapine drugs reached 98% mainly due to the sorption capacity of activated carbons. Thus, pollutants tend to be adsorbed more efficiently on the surface of the composite close to the TiO<sub>2</sub> catalyst. Moreover, TiO<sub>2</sub>/AC composites enhance the generation of superoxide radicals and hydroxyl radicals.

Titanate nanomaterials (especially titanate nanotubes, TNTs) as the carriers of TiO<sub>2</sub> and the adsorbents for heavy metals have attracted great attention from researchers [56]. Because their high specific area, great ion-exchange properties, easy solid–liquid separation and abundant functional groups [57,58]. As the carriers of TiO<sub>2</sub>, titanate nanomaterials can provide lots of nano-scale reactive sites when reacting with contaminants and improve the separation between catalysts and pollutants for the good sedimentation property of titanate nanomaterials [31]. Liu et al. [59] synthesized the TiO<sub>2</sub>/titanate nanosheet composite material (TNS) and used of Cr(VI) and 4-chlorophenol (4-CP) as the target pollutants to tested its performance. The resulted showed that the Cr(VI) removal efficiency attained 99.7% within 120 min and the removal efficiency of 4-CP was 98% within 60 min. They reported that the excellent performance was mainly because the synergetic photocatalysis and autosynchronous doping. The efficiency of the separation between electron-hole pairs was enhanced due to the combination of photo-reduction of Cr(VI) by electrons and photo-degradation of 4-CP by holes. In addition, the adsorption of the reduced Cr(III) by TNS can narrowed energy band gap and enhanced photocatalytic activity of the materials. Zhao et al. [60] constructed the TiO<sub>2</sub> decorated titanate nanotubes composite (TiO<sub>2</sub>/TNTs) and used for photocatalytic degradation of bisphenol A (BPA). They compared the performance of the TiO<sub>2</sub>, TNTs, and TiO<sub>2</sub>/TNTs. The experiment result showed that in the first cycle, the degradation rate of BPA using TiO<sub>2</sub>, TNTs, and TiO<sub>2</sub>/TNTs was 100%, 5.8%, and 94% under UV light. Although the removal efficiency of BPA by TiO<sub>2</sub> is slightly higher than that of TiO<sub>2</sub>/TNTs in the first cycle, reusability of TiO<sub>2</sub>/TNTs was proved in the next cycles. After five reuse cycles, the degradation rate of BPA still reached 91% by using TiO<sub>2</sub>/TNTs and 95.8% of the material could be separated after 6 h gravity-settling, while the 1.8% BPA was removed and 93% of TiO<sub>2</sub> will lose after gravity settling and cannot be reused in pure TiO<sub>2</sub> group. Besides, Li et al. [61], Cheng et al. [62], and Ji et al. [63] also used titanate materials modified TiO<sub>2</sub> to treated the 4-chlorophenol, phenanthrene, and sulfamethazine, respectively.

In addition, many types of polymer materials have been chosen as catalyst carriers, such as polyethylene (PE), polyvinylidene chloride (PVDF), and polyaniline (PANI) Tu et al. [64] incorporated rectorite (REC) into a porous polycaprolactone (PCL)/TiO<sub>2</sub> nanofiber and tested its photocatalytic performance. The results showed that the degradation rate of PCL/TiO<sub>2</sub>/REC to rhodamine B was 98%. Because the porous PCL mats could provide large contact area for TiO<sub>2</sub>. Besides, the addition of rectorite (REC) could reduce the diameters of fibers and enlarge the specific surface area, which might improve the photocatalytic efficiency. Ni et al. [65] fixed nano-TiO<sub>2</sub> nanometers in a polyvinyl alcohol–ethylene–ethylene nanofiber scaffold and tested its photocatalytic performance by using methylene blue (MB) as a target pollutant. The experimental results showed that the degradation rate of MB was 97% in 150 min. Mohsenzadeh et al. [66] synthesized the PANI-TiO<sub>2</sub> nanocomposite using the *n*-situ deposition oxidative polymerization method. The results showed that the material had good photocatalytic degradation performance for 1,2-dichloroethane wastewater because of the large contact area for TiO<sub>2</sub>.

Although non-metallic materials loaded TiO<sub>2</sub> can improve the photocatalytic activity, there are still many problems. High-quality carriers and immobilization methods to complete the photocatalyst loading is necessary. Furthermore, the interaction between carriers and photocatalyst and its effect on catalytic efficiency need to be investigated.

## 2.2. Non-Metal Element Doping Modification

The doping of non-metal elements has always been a hot spot in the field of photocatalytic modification. Doping non-metal atoms can broaden the photoresponse range of TiO<sub>2</sub>. Non-metal

ion doping reconstructs  $\text{TiO}_2$  valence band and moves it upward, which can shorten the gap width (Figure 2).

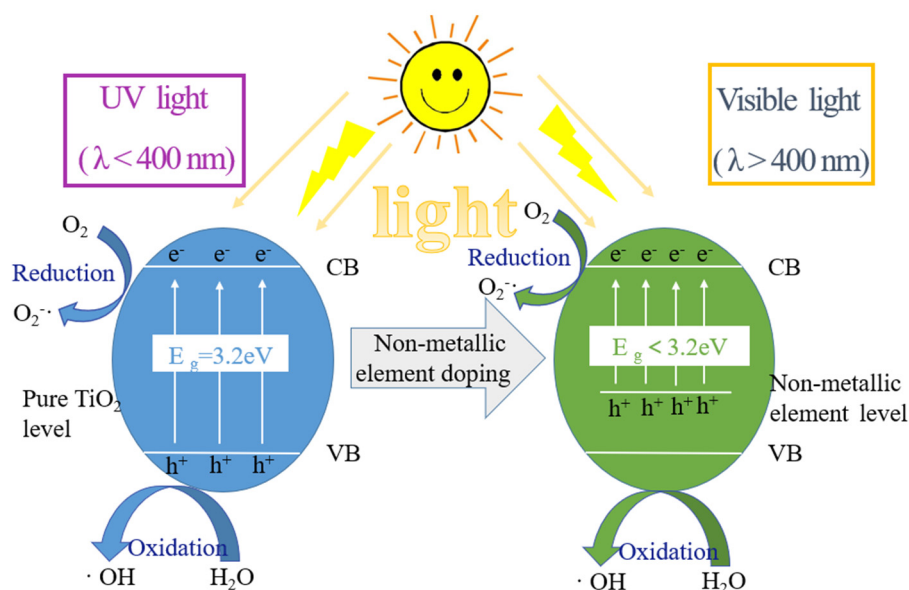


**Figure 2.** The mechanism of non-metallic element doping modification system.

The lifetime of photogenerated electron-hole pairs and the region of light response to visible light are vital for  $\text{TiO}_2$  to increase the value in pollutant treatment [67]. In recent years, it has been found that doping non-metallic elements such as S, N, C, B, I, and F to  $\text{TiO}_2$  successfully extended the optical response range of nano- $\text{TiO}_2$  to the visible light region. Non-metal element doping means that oxygen or partial oxygen in the  $\text{TiO}_2$  was replaced by non-metals. The new energy band was reconstructed and the width of the forbidden band was shortened during doping the non-metal element [68–70]. As a result, the light response range was expanded. Doping non-metallic elements could increase the impurity level in the forbidden band of  $\text{TiO}_2$  and help the band energy level keep higher than the reduction level, where the energy level of  $\text{TiO}_2$  are overlap [71–73]. Asahi et al. [74] first replaced a small amount of lattice oxygen in  $\text{TiO}_2$  with non-metallic element N doping, and successfully achieved visible light catalytic activity of  $\text{TiO}_2$ . The preparation method of non-metal element doped  $\text{TiO}_2$  photocatalyst can be divided into post-treatment and process treatment. Process treatment means that non-metal elements was doped during the formation of  $\text{TiO}_2$ , and post-treatment means that non-metal elements was doped after  $\text{TiO}_2$  formation.

Li et al. [75] prepared N-doped  $\text{TiO}_2$  using the sol-gel method, and the degradation results of dye methylene orange (MO) showed that the degradation rate of pure  $\text{TiO}_2$  was less than 5% after 180 min under visible light, whereas that using N-doped  $\text{TiO}_2$  as the catalyst was over 95% after 90 min. N doping substantially enhanced the ability of  $\text{TiO}_2$  to degrade MO under visible light because N impurity and  $\text{Ti}^{3+}$  acted cooperatively to narrow the band gap of N-doped  $\text{TiO}_2$ . Jyothi et al. [76] prepared N and F co-doped  $\text{TiO}_2$  using the hydrothermal method to remove bromoethane in the solution. The doping element inhibited the photogenerated electron-hole recombination to generate the hydroxyl radical ( $\bullet\text{OH}$ ). The synergistic effect increased the removal rate of bromoethane for 90 min from 54% of pure  $\text{TiO}_2$  to 94%. Rahbar et al. [77] prepared S and N co-doped carbon quantum dots (CQDs)/ $\text{TiO}_2$  composites using the hydrothermal method. The degradation rate of acidic AR88 (azo dyes) under visible light irradiation was 54%, which was higher than that of pure  $\text{TiO}_2$ . They also reported that CQDs allowed the separation of charges due to the electron transport characteristics. In addition, the surface functional group enhanced the photocatalytic activity by providing a higher adsorption capacity on the photocatalyst surface, and pollutant molecules were adsorbed on the photocatalyst surface to promote the photocatalytic reaction. Liu et al. [78] used I-doped  $\text{TiO}_2$  (I- $\text{TiO}_2$ )

material as the electrode of the photoelectrocatalytic method. The experimental results showed that the removal efficiency of diclofenac through modified photoelectrode reached 60%, whereas only 10% was removed using the TiO<sub>2</sub> photoelectrode after 2 h (1.4 V) of visible light. Photoexcited electrons in the conduction band (CB) of TiO<sub>2</sub> can be accepted by the carbon structure due to the high electron storage capacity of carbon materials such as carbon nanotubes. Therefore, the doping of non-metal element not only extends the photocatalytic reaction to visible light, but also improves the photon efficiency of TiO<sub>2</sub> by promoting the separation of charge carriers.

Although doping non-metallic elements improves the visible light response of TiO<sub>2</sub>, the band gap width reduces. As a result, the oxidizing ability of the TiO<sub>2</sub> nanocrystalline phase is directly reduced, and the adsorbed substances cannot be completely degraded. Therefore, the development of non-metal doping remains a hot and difficult issue in the field of photocatalysis.

### 3. Metal Materials Modified TiO<sub>2</sub>

Metal materials such as stainless steel, nickel mesh and nickel foam can be used as carriers for TiO<sub>2</sub> to solve the pollutant problems. However, metals are generally expensive and damage the crystal lattice in some respects. Therefore, metals are hardly used as carriers. Since the surface of metal is similar to that of glass, it generally has poor adhesion and is difficult to load. Hence, precious metal deposition and metal ion doping are mostly used to modify TiO<sub>2</sub>. At present, the metal materials which are used to modify TiO<sub>2</sub> include transition metals (Cr, Fe, and Cu) [79–81], precious metals (Ag, Au, and Pt) [82–84], and rare earth metals (Ce, La, and Nd) [85–87].

#### 3.1. Precious Metal Materials Deposition

Precious metal materials with a large radius are easy to deposit on the surface of TiO<sub>2</sub> particles and can be used as an effective trap for electrons when a certain amount of precious metals is deposited [88–90]. As shown in Figure 3, electrons can transfer from the surface of TiO<sub>2</sub> with a higher Fermi level to the surface of the precious metal with a lower Fermi level. When the Fermi levels of the two surfaces are the same, the electrons will stop transferring and form a Schottky barrier, which can effectively separate photogenerated electron–hole pairs and improve the photocatalytic activity of TiO<sub>2</sub> [70,91,92]. Moreover, depositing an appropriate amount of precious metals on the surface of TiO<sub>2</sub> can broaden the response range of TiO<sub>2</sub> to sunlight and improve the utilization of solar energy, that is, the mechanism of depositing precious metals on the surface of TiO<sub>2</sub> to improve the photocatalytic efficiency changes the surface properties of TiO<sub>2</sub>. As a result, the number of electrons on the surface of TiO<sub>2</sub> is reduced, the separation of photogenerated electron–hole pair is promoted, [93–95] and the photoelectric conversion efficiency is improved. Precious metal deposition can improve photocatalytic performance, but the deposition amount on the metal surface must be controlled within a suitable range. If the deposition amount is very large, the metal may become the center of recombination of electrons and holes, which improves the probability of the electron–hole recombination. Therefore, it is not conducive to photocatalytic degradation [96,97]. Precious metal deposition modification has a high selectivity for photocatalytic degradation of organics [98].

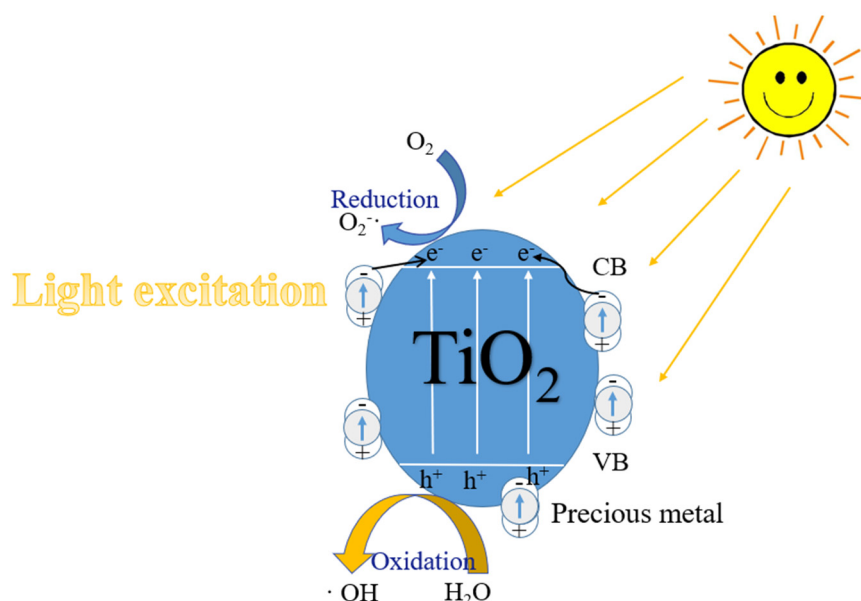


**Figure 3.** The mechanism of precious metal materials deposition.

In the 1980s, Sato et al. [99] reported that Pt deposited on the surface of TiO<sub>2</sub> enhanced the photocatalytic efficiency of water conversion to H<sub>2</sub> and O<sub>2</sub>. Later, Kennedy et al. [100] reported that the incorporation of thermally oxidizable Pt into TiO<sub>2</sub> increased the photocatalytic activity of TiO<sub>2</sub>. The oxidation activity of Pt/TiO<sub>2</sub> was higher than the sum of the oxidizing properties of pure Pt and pure TiO<sub>2</sub>. The improvement was due to the accumulation of holes at the Pt/TiO<sub>2</sub> interface, which led to a decrease in electron-hole recombination in TiO<sub>2</sub>. What is more, the desorption of photo-oxidized intermediated on the surface of TiO<sub>2</sub> and re-adsorption on the surface of Pt with associated thermal oxidation. Ji et al. [101] prepared the Ag-Carbon-TiO<sub>2</sub> composite by using polystyrene/AgNO<sub>3</sub> composite fibers as a sacrifice template. They found that the degradation rate of Rhodamine B reached 90%, when the reaction ran 6 h. Shan et al. [102] synthesized biochar-coupled Ag and TiO<sub>2</sub> composites by mixing, calcination, and photodeposition method. They tested the photocatalytic performance of the material by using methyl orange (MO) as target pollutants. The result shows that TiO<sub>2</sub> modified with Ag showed better photocatalytic degradation performance (the highest decolorization efficiency and mineralization efficiency were 97.48% and 85.38%, respectively) than pure TiO<sub>2</sub>. They attributed the increase in catalytic efficiency to the promotion of the separation of photogenerated electron hole pairs. Jaafar et al. [103] used in-situ electrochemical method to deposit Ag nanoparticles on the surface of TiO<sub>2</sub> and degraded chlorophenol to measure its photocatalytic activity. The study found that Ag-TiO<sub>2</sub> catalyst degraded chlorophenol to 94% after 6 h, for the electron-hole separation had been enhanced.

The precious metal deposition on the surface of TiO<sub>2</sub> achieves a relatively obvious modification effect that significantly increases the degradation rate of some organic compounds. However, the cost of the precious metal deposition method is very expensive and precious metal deposition modified TiO<sub>2</sub> has a high selectivity for photocatalytic degradation of organics, which further limit the application of these materials in pollution treatment.

### 3.2. Metal Ion Doping TiO<sub>2</sub>

Doping different metal ions in TiO<sub>2</sub> photocatalyst is an effective method to improve its catalytic activity [80,104,105]. Metal ions doped with TiO<sub>2</sub> can change the corresponding energy level structure of TiO<sub>2</sub> because metals are more active, and electrons are more easily excited, resulting in a wider range of the absorption in a TiO<sub>2</sub> system [81,106,107]. As shown in Figure 4, metals can capture the electrons generated by TiO<sub>2</sub> excitation, and the electrons inside TiO<sub>2</sub> are not easy to return to the original state.

After metal doping, metal ions can act as a carrier-trapping center, where metal ions higher than tetravalent are more likely to acquire electrons than titanium ions and metal ions lower than tetravalent trap holes. Ion doping can then stop the recombination of electron–hole pairs, which enables TiO<sub>2</sub> to generate more electrons and holes. Thus, the photocatalytic efficiency of TiO<sub>2</sub> is improved [108,109]. For metals with many valence states, electrons in the d orbitals can transition and enter the TiO<sub>2</sub> lattice, which can reduce the band gap and the energy required for the electron transitions [110,111]. This is vital to improve the activity of TiO<sub>2</sub> photocatalyst [112]. The transition group metal ions doped with TiO<sub>2</sub> can change the crystalline morphology and energy level structure of nano-sized TiO<sub>2</sub> to form impurity energy levels [68]. Photons with lower energy can also undergo transitions, thereby expanding their absorption wavelength range and improving the utilization of visible light [113].

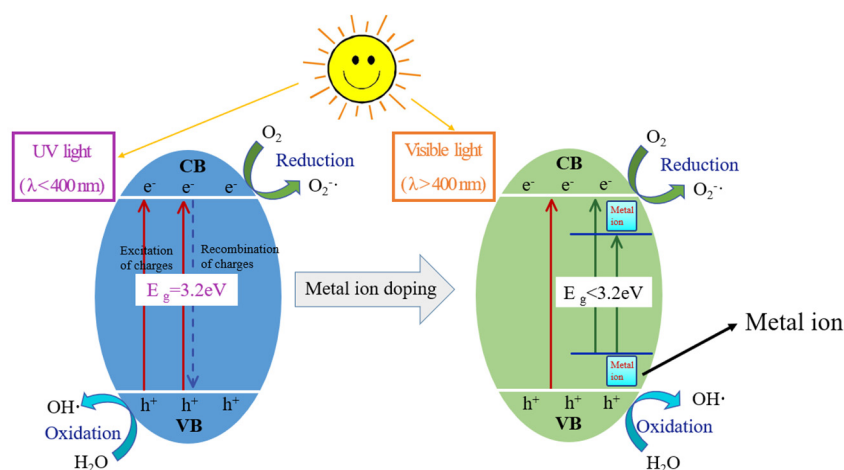


**Figure 4.** The mechanism of metal ion doping TiO<sub>2</sub>.

As early as 1994, Choi et al. [114] began studying the doping of metal ions with TiO<sub>2</sub>. In the experiment, 19 kinds of transition metal ions were doped into nano-TiO<sub>2</sub> and showed a better catalytic activity with the dope of Fe<sup>3+</sup>, Mo<sup>5+</sup>, Os<sup>3+</sup>, and Rh<sup>3+</sup> due to the match of doped ionic potential and radius with TiO<sub>2</sub>. Du et al. [115] used Ge<sup>4+</sup>-doped TiO<sub>2</sub> to prepare Ge/TiO<sub>2</sub> photocatalytic materials and degraded ciprofloxacin. The radius of Ge<sup>4+</sup> was 0.054 nm, which was smaller than that of Ti<sup>4+</sup> (0.068 nm). Ge entered the TiO<sub>2</sub> lattice and replaced the position of Ti, causing lattice defects and delaying the recombination of electrons and holes. Therefore, the formation of •OH on the surface of TiO<sub>2</sub> and the photocatalytic efficiency increased. Degradation rate reached 97% when the calcination temperature was 571 °C and the doping amount was 0.26%. Crisan et al. [116] prepared Fe-doped nano-TiO<sub>2</sub> using the sol-gel method, and the absorption spectrum was extended to 546 nm. Moreover, the corresponding band width at the wavelength of 410 nm was 3.03 eV when the Fe content (w) was 2%. Compared with pure TiO<sub>2</sub>, the degradation rate of nitrobenzene with 0.5% Fe nano-TiO<sub>2</sub> was increased from 70% to 88%. Gnanasekaran et al. [117] found that the spectral absorption range of Co-doped TiO<sub>2</sub> was extended from 382 to 411 nm when the band gap width was reduced to 3.01 eV. The degradation rate of MO after visible light catalytic treatment for 240 min reached 53%, which was beneficial to its photocatalytic performance. Huang et al. [118] used the sol-gel method to prepare Mo-doped nano-TiO<sub>2</sub> powders, and the degradation rate of MB reached 98% under outdoor sunlight with the amount of 2% Mo<sup>6+</sup> (w). This result was mainly due to the reduction of the forbidden band from 3.05 to 2.73 eV with the doping of Mo<sup>6+</sup> and the wider excitation absorption wavelength. Bhatia and Dhir [112] made Ni-TiO<sub>2</sub> and Bi-TiO<sub>2</sub> using the sol-gel method and found that the maximum degradation rate of ibuprofen by Bi-TiO<sub>2</sub> and Ni-TiO<sub>2</sub> reached 89% and 78%, respectively. This finding may be attributed to the increase in specific surface area and the decrease in the crystallite size. Wang et al. [119] prepared an Fe<sup>3+</sup>-doped TiO<sub>2</sub> nanotube array catalyst using a simple hydrothermal method, which increased

the degradation rate of MB by about 20%. The study also found that  $\text{Fe}^{3+}$  doping provided traps in the  $\text{TiO}_2$  lattice, which greatly improved the separation effect of electron–hole pairs.

#### 4. Composite Materials Modified $\text{TiO}_2$

##### 4.1. The Construction the Heterojunction

The heterojunction is a contact interface, formed as a result of hybridization between two semiconductors [120,121]. The semiconductors used for the heterojunction need to satisfy the condition that they should exhibit different band gaps and the narrow band gap must lie in the visible region [122]. Combining  $\text{TiO}_2$  with other semiconductors to construct heterojunction can efficiently improve the photocatalytic performance of  $\text{TiO}_2$  [123,124]. This method can not only improve the effective utilization rate of the electrons by promoting the photo-generated electrons and holes to transfer in the opposite direction but also expand the spectral response range of the composite to visible light and even near infrared region [125–127]. Generally, the most widely researched types of the  $\text{TiO}_2$ -based heterojunction can be categorized into two different types depending on the charge carrier separation mechanism, which are conventional type and direct Z-scheme [128–130].

Based on the different band and electronic structures, the conventional type can be divided into three, namely, type-I (straddling gap), type-II (staggered gap), and type-III (broken gap) heterojunctions [131,132]. For type-I heterojunctions, the level of the CB of semiconductor-I is higher than that of semiconductor-II, while the valence band (VB) of semiconductor-I is lower than that of semiconductor-II. However, due to the difference between the band gaps, the photoinduced charges accumulate on smaller band gap semiconductor, which may cause recombination. In type-II heterojunctions (Figure 5b), the level of CB and the VB of semiconductor-II are higher than those of semiconductor-I [133]. In addition, the migration of charge carriers to the opposite directions can be promoted because the difference between the chemical potentials causes a phenomenon called band bending. The band structure of the type-III heterojunctions (Figure 5c) is similar to that of type-II except that the staggered gap becomes so wide that the bandgaps do not overlap [134]. Among these conventional heterojunctions, type-II heterojunction attracts the attention of more researchers [135–137]. Ganguly et al. [138] synthesized type-II heterojunctions of the  $\text{AgBiS}_2\text{-TiO}_2$  composite and used doxycycline as the target pollutant to test photocatalytic performance. The results showed that the degradation rate reached 100% in 180 min under a 500 W Xe lamp. The enhanced photocatalytic activity was attributed to the decreased rate of recombination of the photogenerated excitons. Liu et al. [139] used other semiconductors such as  $\text{Bi}_2\text{MoO}_6$  and  $\text{TiO}_2$  to fabricate type-II heterojunctions and tested the photocatalytic performance of  $\text{Bi}_2\text{MoO}_6/\text{TiO}_2$ . They reported that the degradation rate of ciprofloxacin, tetracycline, and oxytetracycline reached 88%, 78%, and 78%, within 150 min, respectively, when the 350 W Xe lamp with a 420 nm cutoff filter was used as the light. The CB of  $\text{TiO}_2$  can serve as the electron transfer platform, which can improve the efficiency of the separation of photocarriers at  $\text{Bi}_2\text{MoO}_6/\text{TiO}_2$  heterojunction interface.

In 2013, the concept of the direct Z-scheme photocatalyst was first proposed [140]. Figure 5d is the band arrangement and electron migration mechanism of Z-scheme heterojunctions. The Z-scheme heterojunctions have the same band arrangement as the type-II heterojunctions, but the electron transfer path between semiconductors is different [141]. The electron transfer path between semiconductors is like the English letter “Z” [142]. In the process of photocatalytic reaction, the photogenerated electrons with lower reduction ability in semiconductor-II recombine with the photogenerated holes in semiconductor-I with lower oxidation ability. Therefore, the photogenerated electrons with high reduction ability in semiconductor-I and the photogenerated holes with high oxidation ability in semiconductor-B can be maintained [143]. In addition, the electrostatic attraction between the photogenerated electron on the CB of the semiconductor-II and the photogenerated holes on the VB of the semiconductor-I will promote the migration of the photogenerated electron from the semiconductor-II to the semiconductor-I, while in the type-II heterojunction, the electrostatic repulsion

between the photogenerated electron of the semiconductor-I and the semiconductor-II will inhibit the transfer of electrons from semiconductor-I to the semiconductor-II [144,145]. So far, many photocatalytic composites that have the Z-scheme heterojunctions have been manufactured to degrade the pollutants. Wang et al. [146] fabricated the N-doped carbon quantum dot (NCDs)/TiO<sub>2</sub> nanosheet with higher surface energy faceted (NCDs/TNS-001) composites and used diclofenac (DCF) as the target pollutants. The photocatalytic efficiency of the composites reached 92% in 60 min under the 350 W Xe lamp. In contrast, only 15.4% of the DCF was degraded in the presence of TNS-001 after 60 min. They reported that the excellent photocatalytic performance might be attributed to the synergistic effects of the highly active facets, up-converted fluorescent properties of NCDs, and efficient charge separation induced by fabricated Z-scheme heterostructures. Hao et al. [147] used the TiO<sub>2</sub>@g-C<sub>3</sub>N<sub>4</sub> core-shell photocatalysts with the Z-scheme heterojunctions to remove the Rhodamine B from water. The removal efficiency under the 100 Xe lamp was about 96% within 180 min, while the Rhodamine B (RhB) dye shows almost no degradation in the blank test. They attributed the improvement of photocatalytic performance to the formation of the Z-scheme system, which effectively separated photogenerated electrons and holes. Liao et al. [148] prepared a photocatalytic material g-C<sub>3</sub>N<sub>4</sub>-Ti<sup>3+</sup>/TiO<sub>2</sub> nanotube arrays and tested its performance of degrading the phenol. At a reaction period of 7 h, the degradation was only 23.4% using TiO<sub>2</sub> nanotube arrays, while the degradation rate increased to 74% using the g-C<sub>3</sub>N<sub>4</sub>-Ti<sup>3+</sup>/TiO<sub>2</sub> nanotube arrays. This was mainly because that the self-doping of Ti<sup>3+</sup> promoted the visible light absorption behavior of the composite and the Z-scheme heterojunctions with efficient space separation of the photo-generated electron-hole.

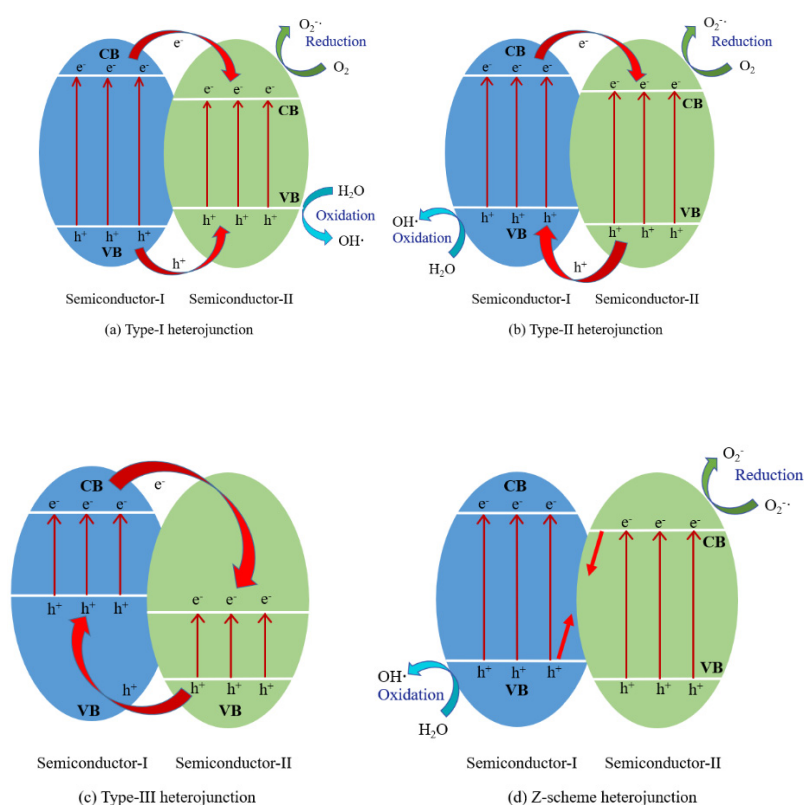


**Figure 5.** The band arrangement and electron migration mechanism of different heterojunctions. (a) Type-I heterojunction; (b) Type-II heterojunction; (c) Type-III heterojunction; (d) Z-scheme heterojunction.

Semiconductor heterojunction powders have exhibited the enhanced photocatalytic activities, but their practical applications have been limited due to their poor recycling performance from flowing wastewater.

#### 4.2. Different Elements Co-Doping TiO<sub>2</sub>

The emphasis of single element doping on the modification of TiO<sub>2</sub> is different. In order to improve the migration range of absorption edge, photocatalytic performance and thermal stability of TiO<sub>2</sub> at the same time, the co-doping of multiple elements is an ideal solution [149]. Co-doped nanoparticles exhibit higher visible light absorption than single doped TiO<sub>2</sub> due to a synergistic effect between the two dopants, which can efficiently increase the photocatalytic performance [150]. Co-doping can be divided into different metal elements co-doping [151–153], metal elements and non-metal elements doping [154–156] and different non-metal elements doping [157–159]. As shown in Table 2, many researchers have used co-doping method to modify TiO<sub>2</sub> and tested the photocatalytic performance of the materials.

**Table 2.** The photocatalytic performance of the co-doped TiO<sub>2</sub> in treating pollutants.

Doping Elements	Crystal Phases of TiO <sub>2</sub>	Light Source and Reaction Time	Target Pollutant	Degradation Rate	Ref.
Ni, Cr	anatase	Sunlight 90 min	methylene blue	96%	[153]
Cu, Co	anatase	LED 300 min	acetaldehyde	99%	[160]
Ag, V	-	40 W white light bulbs 180 min	hexane gas butyl acetate gas	94% 96%	[161]
N, Cu	anatase	200 W Xe lamp 60 min	sulfamethoxazole	99%	[162]
Fe, I	anatase	visible light 60 min	gaseous benzene	59%	[80]
Mn, N	anatase, rutile, wurtzite	LED 40 min	Quinalphos 2-chlorophenol	92% 88%	[163]
N, Ag	anatase	LED 360 min	methylene blue	99%	[164]
Ag, Pd, N	anatase	mercury vapor lamp 120 min	malachite green methylene blue mongo red	75% 92% 62%	[165]
C, N	anatase	simulated sunlight 420 min	4-nitrophenol	87%	[166]
N, F	anatase	500 W Xe lamp 150 min	methylene blue	89%	[167]
Si, N	anatase	500 W Xe lamp 180 min	Rhodamine B	86%	[168]
C, N	anatase and rutile	300 W Xe lamp 150 min	phenol	92%	[169]

At present, the physical and chemical properties and the doping mechanism of co-doped TiO<sub>2</sub> with two different metals have not been thoroughly investigated. Singh et al. [170] synthesized the mesoporous La-Na co-doped TiO<sub>2</sub> nanoparticles (NPs). The removal efficiency of MB was almost 100% by using the Na and La doped TiO<sub>2</sub>, while 35% MB was degraded by using pure TiO<sub>2</sub> mainly because of the substitution of large-sized Na<sup>+1</sup> and La<sup>+3</sup> at Ti<sup>+4</sup> sites which was confirmed by the results of XRD and TEM. The doping of these low-valent metal ions led to the formation of O vacancies, which promoted the adsorption of hydroxyl groups on the surface of NPs. The adsorbed hydroxyl group reduced the pH<sub>IEP</sub>, which was beneficial to the adsorption of cationic MB dyes. Metal components prefer to substitute for the Ti site in the TiO<sub>2</sub> lattice to create the dopant level near the CB. Non-metal components can form new levels closest to the VB that reduce the band gap and cause visible light absorption. Therefore, metal and non-metal ion co-doping enhance photocatalytic activity [163,171]. Garg et al. [172] tested the photocatalytic performance of prepared N and Co-co-doped TiO<sub>2</sub> on the removal of Bisphenol-A under visible light. The results showed that the maximum degradation rate

(95%) was observed when using 1.5% Co and 0.5% N co-doping TiO<sub>2</sub>. This result was almost twice that of the group using pure TiO<sub>2</sub>. TiO<sub>2</sub> was enhanced because Co and N disturbed the physical properties of the nano particles, producing alterations in crystal structure and energy band gap as well as elemental composition. N could easily substitute O in the TiO<sub>2</sub> lattice owing to its atomic size comparable with that of O, and N had small ionization energy and high stability. In addition, the doping of a range of Co could shift the optical absorption edge from UV to visible light range, and Co could behave as recombination centers for the photoinduced charge carriers, thereby decreasing quantum efficiency. Non-metal co-doped TiO<sub>2</sub> have been studied extensively [173–175]. Zeng et al. [176] prepared B/N co-doped TiO<sub>2</sub> photocatalysts and compared their photocatalytic performance with pure TiO<sub>2</sub> under simulated sunlight by using flumequine (FLU) as the target compound. The results showed that the degradation rate of FLU by B/N co-doped TiO<sub>2</sub> was nearly 100%, whereas that of pure TiO<sub>2</sub> was only about 10%. The photocatalytic performance of TiO<sub>2</sub> catalyst was evidently enhanced by B/N co-doping. The relative content of rutile in B/N co-doped TiO<sub>2</sub> catalysts increased with the increase of the B content, which produced a synergistic effect between anatase and rutile. This synergistic effect can be explained by the formation of a semiconductor junction between the anatase phase and the rutile phase, which promoted the separation of photogenerated electrons and holes, thus improving photocatalytic activity.

The method of co-doping can effectively improve the removal efficiency of pollutants by TiO<sub>2</sub>. But some of the elements are not suitable for practical use, so it is necessary to find suitable doping materials. And it is essential to find an optimum amount of dopant to increase the separation of charge carriers and prevent the formation of a recombination center.

#### 4.3. Dye Photosensitization

Dye photosensitization means that the photosensitizer (dyes) binds to TiO<sub>2</sub> surface by chemical or physical adsorption, so that the absorption wavelength of visible light shifts to the long wavelength, thus expanding the excitation wavelength response range of TiO<sub>2</sub> and greatly improving the utilization of sunlight [177–179]. The molecule (dyes) absorbing the photon is called as a photosensitizer and the altered material (TiO<sub>2</sub>) is the acceptor or substrate [180]. As shown in Figure 6, the mechanism of photosensitization is that once the dyes achieve their excited state by the absorption of photons in the visible range of the solar spectrum, electrons from the dyes' highest occupied molecular orbital (HOMO) are transferred to their lowest unoccupied molecular orbital (LUMO) and subsequently to the conduction band (CB) of TiO<sub>2</sub> [181–183]. In addition, the dyes in solution can be excited to a triplet state under visible light and transfer their excess energy to the O<sub>2</sub>. Thus, the electrons in the LUMO react with dissolved oxygen and produce the superoxide anion radical [184]. Dyes used for photosensitization must meet the following characteristics: strong absorption of visible light even the part of the near infrared (NIR) region, photo stability (unless the self-sensitized degradation is required), the existence of some anchoring groups (-SO<sub>3</sub>H, -COOH, -H<sub>2</sub>PO<sub>3</sub>, etc.) and the higher excited state energy than the conduction band (CB) edge of TiO<sub>2</sub> [185,186]. According to the composition, dyes can be divided into two categories: organometallic dyes and organic dyes. Organometallic dyes contain a transition metal in the structure and the organic dyes are composed of organic chromophores [187].

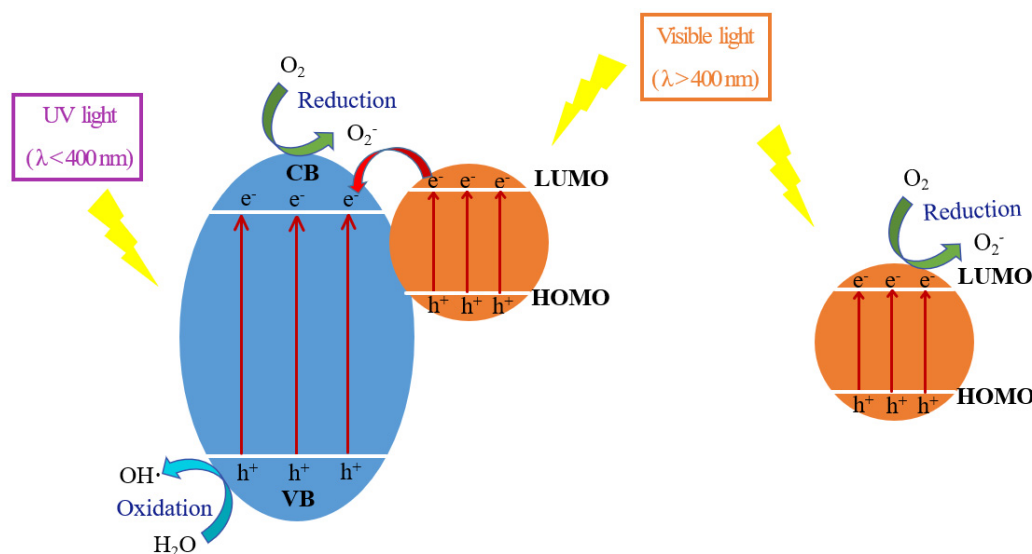


**Figure 6.** The mechanism of the dye sensitization process.

Ahmad and Kan [188] used a phthalocyanine-based reactive dye, C.I. reactive blue 25 (RB-25), as a dye photosensitizer for anatase ( $\text{TiO}_2$ ) and tested photocatalytic performance by degradation of Rhodamine B (RhB). The result showed that RhB was relatively stable under visible light in the presence of only  $\text{TiO}_2$ . Degradation rate reached more than 90% when the RB-25 dye was adsorbed on the  $\text{TiO}_2$  mainly because the electrons from the dye increased the electron density in the CB of the  $\text{TiO}_2$ , which enhanced photocatalytic activity under visible light. Mucria et al. [189] modified  $\text{TiO}_2$  by dye sensitization. The photosensitizers applied were quinizarin and zinc protoporphyrin. The result showed that the removal efficiency of both exceeded 80%. The improvement of their activity could be ascribed to the presence of sensitizing molecules within the nanotubes, whose electronic properties were promoted by the electron confinement effect in semiconductors. Moreover, electron–hole recombination rate for this material in comparison to the higher surface materials because the electrons can initially reach the dye before the CB. Sensitized materials can also be used for desulphurization. Guo et al. [190] loaded  $\text{TiO}_2$  onto SBA-15 molecular sieves and sensitized with organic dyes (2,9-dichloroquinacridone, DCQ) to extend its spectral response range from ultraviolet light to visible light. The material was then applied for the photocatalytic oxidation desulfurization of gasoline. Experimental results showed that DCQ- $\text{TiO}_2$ @SBA-15 performed better than unsensitized  $\text{TiO}_2$ @SBA-15, and desulfurization rate can reach 96.1% in a reaction time of 90 min.

The modification method of photosensitization can greatly improve the photocatalytic performance of titanium dioxide. However, there are still some problems need to be solved. For example, the organic dye molecule will gradually degrade due to the photocatalytic. So, it is necessary to replace the catalyst continuously. Additionally, the absorption of most photosensitizers is weak in the near-infrared region and there is adsorption competition with pollutants, which limits the development of photosensitization. Therefore, further research is needed to solve these problems.

## 5. Application of Modified $\text{TiO}_2$ Composite Photocatalytic Materials

Photocatalytic treatment technology is the most representative advanced oxidation technology for environmental pollution treatment. It uses the hydroxyl radical ( $\bullet\text{OH}$ ) as a strong oxidant to deeply oxidize and decompose organic pollutants into non-toxic inorganic small molecules [191]. At the same time, the photocatalytic reduction reaction can effectively remove heavy metal ions. Table 3 is the performance of the modified  $\text{TiO}_2$  in treating pollutants.

**Table 3.** The performance of the modified TiO<sub>2</sub> in treating pollutants.

Photocatalysts	Crystal Phases of TiO <sub>2</sub>	Light Source and Reaction Time	Target Pollutant	Degradation Rate	Ref.
TiO <sub>2</sub> /biochar	anatase	500 W mercury lamp 150 min	methyl orange	97%	[192]
Fe <sup>3+</sup> -TiO <sub>2</sub> nanoparticles	anatase	150 W Xe lamp 240 min	4-chlorophenol ethyl orange	65% 95%	[193]
TiO <sub>2</sub> -Fe-porphyrin-conjugated microporous polymers	anatase	Xe lamp 90 min	methyl orange	96%	[194]
Gd-TiO <sub>2</sub>	anatase	visible light 93 min	methylene blue	28%	[195]
polypyrrole@TiO <sub>2</sub>	anatase and rutile	250 W mercury lamp 60 min	methylene blue	25%	[196]
W, F-TiO <sub>2</sub>	anatase	500 W halogen lamp 180 min	methylene blue	96%	[197]
sodium borosilicate glass SiO <sub>2</sub> -B <sub>2</sub> O <sub>3</sub> -Na <sub>2</sub> O- ZnO with CdS and TiO <sub>2</sub>	anatase	Sunlight 300 min	indigo carmine dye	92%	[198]
TiO <sub>2</sub> -ZrTiO <sub>4</sub> -SiO <sub>2</sub>	anatase	300 W Xe lamp 90 min	rhodamine B	95%	[199]
TiO <sub>2</sub> -W <sub>18</sub> O <sub>49</sub>	anatase	visible light 60 min	rhodamine B	82%	[200]
C/Fe-TiO <sub>2</sub> coated on activated carbon terephthalic acid functionalized	anatase	36 W compact light 140 min	rhoda mine B	99%	[201]
g-C <sub>3</sub> N <sub>4</sub> /TiO <sub>2</sub> /Fe <sub>3</sub> O <sub>4</sub> @SiO <sub>2</sub>	anatase	8 W compact fluorescent lamps 120 min	ibuprofen	97%	[202]
Cu-TiO <sub>2</sub>	anatase	500 W Xe lamp 140 min	formaldehyde	100%	[203]
MIL-101(Fe)/TiO <sub>2</sub>	anatase	Sunlight 30 min	tetracycline	93%	[204]
WO <sub>3</sub> /TiO <sub>2</sub>	anatase	500 W Xe lamp 60 min	paracetamol	100%	[205]
MoS <sub>2</sub> /TiO <sub>2</sub> /Carbon Fiber	rutile	visible light 60 min	tetracycline	93%	[206]
Bi <sub>2</sub> S <sub>3</sub> /TiO <sub>2</sub> /Montmorillonite	anatase	mercury vapor lamp 120 min	ketoprofen	90%	[207]
TiO <sub>2</sub> -reduced graphene oxide (TiO <sub>2</sub> -rGO)	anatase	simulated sunlight 90 min	formalin	98%	[208]
TiO <sub>2</sub> /glass	anatase	Sunlight 30 min	2,5-dichlorophenol	95%	[209]
Bi, B-TiO <sub>2</sub>	anatase	Xe lamp 90 min	5-fluorouracil	100%	[210]
Ce, Mn- TiO <sub>2</sub>	anatase	30 W ultraviolet lamp 240 min	diclofenac	94%	[211]
Fe-TiO <sub>2</sub>	anatase and rutile	visible light 1050 min	acetaldehyde	65%	[212]
N, F-TiO <sub>2</sub>	anatase	mercury vapor lamp 180 min	ethylbenzene	33%	[213]
activated carbon-TiO <sub>2</sub>	anatase and rutile	UV light 20 min	toluene	99%	[214]
Eosin Y- TiO <sub>2</sub>	anatase	visible light 180 min	acetaminophen diclofenac	71% 83%	[185]
Cu-TiO <sub>2</sub> combine with activated carbon fiber	anatase and rutile	fluorescent lamp 180 min	Benzene toluene	81% 98%	[215]

### 5.1. The Application in Water Pollution

Wastewater treatment plants can remove a large majority of the pollution. However, several trace organic compounds or refractory compounds cannot be degraded by the conventional treatment [216]. These pollutants mostly result from domestic and industrial use of pharmaceutical preparations, printing and hygiene products, and pesticides. In recent years, photocatalytic technology has broadened its application in the treatment of organic wastewater. Under the conditions of sufficient O and light, TiO<sub>2</sub> uses the photogenerated electrons and holes to degrade almost all organic pollutants in water and convert them into CO<sub>2</sub>, H<sub>2</sub>O, and other inorganic substances. Saif et al. [217] prepared lanthanide (Nd<sup>3+</sup>, Sm<sup>3+</sup>, Eu<sup>3+</sup>, Gd<sup>3+</sup>, Dy<sup>3+</sup>, and Er<sup>3+</sup>)-doped TiO<sub>2</sub> using the sol-gel method and evaluated their photocatalytic activity in the treatment of actual sewage. In the actual sewage treatment plant application, the mineralization efficiency of Gd<sup>3+</sup>-TiO<sub>2</sub> and Eu<sup>3+</sup> TiO<sub>2</sub> on chemical oxygen

demand (COD) reached 67% and 50%, respectively, after 6 h of light. Lima et al. [218] used Ag/TiO<sub>2</sub> photocatalytic material to degrade the hormones which would exist in the sewage treatment plant. The results showed that the degradation rate of the hormone by Ag/TiO<sub>2</sub> reached 95% after 3.5 h. In addition to organic pollutants, photocatalytic technology can achieve better treatment of inorganic substances in water. Peng et al. [219] prepared TiO<sub>2</sub>-CuO/HSC composites. Degradation rates of ammonia nitrogen in water reached 61% and 100% when experiments were operated under ordinary light and ultraviolet light, respectively.

Dyeing wastewater discharged from printing and dyeing factories contains a large number of dye molecules. These dye molecules usually contain a mine groups, aromatic rings, azo groups, etc. Therefore, the chromaticity of dye wastewater is difficult to meet standards for discharge. Traditional biological and physical treatment methods for removing organic pollutants, which include precipitation, adsorption, flocculation, reverse osmosis, and ultrafiltration, are inefficient and unsuitable for industrial applications. So, people choose photocatalytic degradation as an alternative technology to solve the pollutants [220–222]. TiO<sub>2</sub> can not only effectively remove the color of wastewater, but also decomposes the pollutants into small molecules such as CO<sub>2</sub> and H<sub>2</sub>O. Xu et al. [223] successfully prepared Ag/TiO<sub>2</sub> layered structure and reported the degradation rate of the dye under the sunlight reached 99%, while the degradation rate of pure TiO<sub>2</sub> was 43%. Ji et al. [224] used C/TiO<sub>2</sub> microsphere to degrade the rhoda mine B. The results showed the degradation rate of rhoda mine B reached 96% within 140 min, and the degradation rate still maintained above 80% after the material was used for three times. Fu et al. [225] use graphene oxide/TiO<sub>2</sub> (GO/TiO<sub>2</sub>) composites to degrade the dyes and reported the degradation rate of the dyes reached 96% within 2.5 h.

Tannery wastewater is also a major problem in industrial wastewater because of the containing of large amounts of poorly biodegradable organic chemicals. The general biological treatment method can make the effluent reach the standard, but it still needs multiple treatments to remove most of the COD, color and some organic recalcitrant compounds. So, the photocatalytic treatment using TiO<sub>2</sub> become a new method to treat tannery wastewater. He et al. [226] used Mn-doped TiO<sub>2</sub> material to degrade the tannery wastewater. The degradation rate of organic pollutants under sunlight was nearly 90%. Bordes et al. [227] deposited the fine-structured photocatalytic TiO<sub>2</sub> coatings on austenitic stainless steel coupons by atmospheric plasma spraying (APS) and the total organic carbon (TOC) removal reached 49%, while the decolorization rate reached 75%. Therefore, they reported that the decreased TOC and color removal of the resulting effluent evidenced the effectiveness of the developed coatings for photocatalytic treatment of industrial tannery wastewater.

The large-scale use of pesticides such as herbicides and insecticides have a significant impact on aquatic environment. The harmful effects of these compounds are due to their toxicity and high mobility and persistence in aqueous media [228]. In fact, only a small part of the applied pesticides can protect agricultural products, while most pesticides are lost to the environment through volatilization, hydrolysis, photolysis, or degradation by microbial action [229]. The characteristics of pesticide wastewater lead to ineffective treatment by physical and biological methods, so photocatalytic oxidation is used to treat this type of wastewater, for example organophosphorus pesticides can be mineralized and decomposed by TiO<sub>2</sub> and converted into non-toxic CO<sub>2</sub>, H<sub>2</sub>O, and PO<sup>4-</sup>. Abdennouri et al. [230] prepared a nano-TiO<sub>2</sub> supported on pillared clay and found that the material can efficiently degrade 2,4-dichlorophenoxyacetic acid, 2,4-dichlorophenoxypropionic acid, and other pesticides in the environment. Both of the degradation reached about 80%.

As an important component of energy, petroleum plays a decisive role in the sustained and rapid development of the national economy. Due to river convergence and marine accidents, a large amount of low-density and water-insoluble oil flows into the ocean every year, causing marine oil pollution and threatening to marine life. Traditional processing is performed by mechanical methods, and biological processes are often used as auxiliary processing steps, followed by advanced processes such as adsorption, membrane filtration, and reverse osmosis. However, due to the presence of high concentrations of toxic aromatic and aliphatic hydrocarbons in addition to the presence of phenols and

refractory compounds, the biological processes cannot meet the standard of reuse [231,232]. Studies have shown that TiO<sub>2</sub> photocatalysts can float on the water surface and are efficient in the degradation of toxic and recalcitrant pollutants [233]. Shivaraju et al. [234] prepared N-doped TiO<sub>2</sub>. They reported the degradation rate of oil and grease and other organic pollutants in wastewater can reach about 90%.

The pollution of pharmaceuticals in industrial wastewater is serious problem. Traditional wastewater treatment removes most of the pollutants through sedimentation, filtration, adsorption, or biological processes, however, bio-toxic and non-degradable organics usually remain in the water at concentrations above the ppb discharge or reuse limit [235]. Using TiO<sub>2</sub> for photocatalytic reaction would be a good method to solve this problem. Solís-Casados et al. [236] used Sn-doped TiO<sub>2</sub> to treat diclofenac, paracetamol, and ibuprofen under visible light. The results showed the maximum removal rate of diclofenac was 25%, the maximum removal rate of paracetamol was 25%, and the removal rate of ibuprofen was 18%. All of the three drugs were effectively reduced. Malakootian et al. [237] used Fe<sup>3+</sup> doped TiO<sub>2</sub> materials to degrade pharmaceutical wastewater and antibiotic-added synthetic solutions. The results showed that the degradation rates of antibiotics can reach 70% and 97%, respectively. Besides, Lcerda et al. [238] and Hou et al. [239] also used the TiO<sub>2</sub> to degrade the pharmaceutical wastewater and obtained satisfied result.

### 5.2. The Application in Air Pollution

Cars provide convenience for people's travel, but the automobile exhaust gas seriously affects air quality and endangers people's health. NO<sub>x</sub> in automobile exhaust not only stimulates the human respiratory system, but also causes problems such as acid rain and photochemical smog. So, the removal of NO<sub>x</sub> has attracted people's attention. However, the traditional technologies of NO<sub>x</sub> removal, including physical adsorption and selective catalytic reduction, cannot remove the NO<sub>x</sub> effectively at ppb levels [240,241]. TiO<sub>2</sub> photocatalyst provides an effective way to solve these problems by mixing in paint, concrete and brick or fixing on the surface of roads and walls. Under sunlight, the TiO<sub>2</sub> photocatalyst can oxidize NO<sub>x</sub> to form nitric acid through a series of reactions. Then the nitric acid reacts with the components fixed the photocatalyst to obtain nitrate. Under the action of rainwater, nitrate ions are formed and washed away. Zhang et al. [242] found that nano-TiO<sub>2</sub>/diatomite composites efficiently degraded formaldehyde in the air, showing a good application prospect. Qin et al. [243] found that loading nano-TiO<sub>2</sub> in concrete during road construction could absorb NO<sub>2</sub> in locomotive exhaust, thereby reducing air pollution.

Besides, most volatile organic compounds (VOCs) in air (aldehydes, ketones and alcohols) are oxidizable, it is feasible to remove them by oxidation method. Most of the heterogeneous catalytic oxidation methods commonly used to remove pollutants in the air at high temperatures, which limits the application. Therefore, the photocatalysis method has become a potential method to remove air pollutants by using water vapor and O<sub>2</sub> in air at room temperature with low energy consumption [244,245]. Lai et al. [246] prepared Bi-TiO<sub>2</sub> to degraded toluene and the degradation rate increased by 77% in terms of CO<sub>2</sub> production, as compared to the pure TiO<sub>2</sub>. Rao et al. [247] used Er<sup>3+</sup> doped TiO<sub>2</sub> and reported the modified TiO<sub>2</sub> exhibited higher photoactivity in comparison with the pure TiO<sub>2</sub>. The highest removal efficiency of acetaldehyde and o-xylene within 100 min was 99% and 85%, respectively, and ethylene degradation efficiency reached 22% within 180 min.

### 5.3. The Application in Soil Pollution

There are many types of soil pollutants, which are characterized by the coexistence of emerging and old pollutants. These pollutants include heavy metals, pesticides, antibiotics, and persistent organic compounds, which makes it difficult to get an efficient repair result in soil. Heavy metal pollution and organic pollution are regarded as the main types of soil pollution because of the large amount among the pollutants [248]. The surface of the contaminated soil with a high concentration of pollutants can easily enter the atmosphere or water under the action of wind and water, respectively, leading

to other secondary environmental problems such as air pollution, surface water and groundwater pollution [249–251]. Therefore, soil remediation is imminent.

The pollutants' treatments in soil mainly include physical–chemical remediation technology, biological remediation technology, and phytoremediation technology, but all of these have some shortcomings. The photocatalytic technology can completely mineralize the organic pollutants and remove the heavy metals in the soil. This technology also has the advantages of fast decomposition rate, no secondary pollution, and easy operation [252–254]. In recent years, photocatalysis has been widely used in organic soil remediation studies, including organic pesticides, aromatic organics, petroleum hydrocarbons, and heavy metals [255,256].

TiO<sub>2</sub> is the most widely used catalyst in photocatalyst technology, and it also acts as a key role on pollutants in soil. Kuang et al. [257] reported that the Cd(II) removal efficiency of biological soil crusts increased by 27% than that of pure biological soil crusts after the addition of nano-TiO<sub>2</sub>. They reported that in the first 30 min, the adsorption rate of BSC + TiO<sub>2</sub> composite was faster than that of pure TiO<sub>2</sub>, which may be due to the high adsorption rate of nano-TiO<sub>2</sub>. Petroleum-contaminated soil is highly toxic, and photocatalytic degradation using TiO<sub>2</sub> can also get the ideal results. Yang et al. [258] pretreated the soil with ultraviolet radiation C (UVC) activated TiO<sub>2</sub> under varying moisture conditions to enhance biodegradation of heavy hydrocarbons (HCCs). They reported that total petroleum hydrocarbon (TPH) removal after 24 h exposure to UVC was about 20% in slurries with 300% water holding capacity. In a 10 d bioremediation test, TPH removal in treated soil increased to 27%, compared to 15% for controls without photocatalytic pre-treatment. The improvement mainly because the recalcitrant hydrocarbons were transformed into more bioavailable and biodegradable products so that the pollutants were more readily consumed by soil microorganisms.

Soil remediation of modified TiO<sub>2</sub> has achieved some effects in heavy metal pollution and organic pollution, but there are still some problems, including the insufficient light penetration and difficulty in recycling. Therefore, it is necessary to find TiO<sub>2</sub> composite materials that can make fuller use of sunlight in the soil or improve the recycling rate.

## 6. Conclusions and Perspective

Despite the substantial progress in TiO<sub>2</sub>, considerable opportunities and challenges remain. The synthesis and improvement of TiO<sub>2</sub> has become a hot topic to improve the efficiency of environmental treatment. This review comprehensively discusses several synthesis and doping technologies of TiO<sub>2</sub>, and the effect of each improvement method. Moreover, it elaborates and prospects the application of TiO<sub>2</sub>-modified materials in the environmental field, especially for water, air, and soil pollution.

Developing a pollutant treatment with visible light-responsive photocatalysts is very urgent and necessary. The photocatalytic performance of TiO<sub>2</sub> can be greatly improved through the modification of TiO<sub>2</sub>. However, many problems in application remain to be solved: (i) in many studies, the system has only one kind of pollutant, which does not match the complex multiple components of the actual pollutants. Gaps exist between material research and application studies for practical application. Whether modified TiO<sub>2</sub> can perform well is unknown. Although modified TiO<sub>2</sub> shows potential in the treatment of pollutants, most of the works considered in the scope of this review were carried out on a laboratory scale. (ii) The recycling or natural degradation of the modified materials remains an issue. Few studies were devoted to separation, recovery, and reuse of photocatalytic materials for the treatment of the real pollutants. (iii) Introduction of other materials into TiO<sub>2</sub> will cause the preparation complexity and cost to increase. Materials used for modification may pollute the environment, such as in modification with heavy metal ions or harmful organic.

Future research should focus on the following aspects to improve the applicability and feasibility of the modified TiO<sub>2</sub>: (i) more pilot experiments using modified TiO<sub>2</sub> should be performed for photocatalytic degradation of real pollutants in water, air, and soil. An understanding of inherent charge transfer dynamics and photocatalytic mechanisms at the nanometer and atomic level will be highly useful in designing effective approaches for enhancing the photocatalytic performance of

TiO<sub>2</sub>. Thus, researchers should understand the mechanism of dealing with actual pollutants. (ii) The efficiency and photostability of the modified TiO<sub>2</sub> must be improved. The performance of modified TiO<sub>2</sub> is currently limited by the physicochemical properties of these materials. (iii) Materials used to modify TiO<sub>2</sub> that cause low harm to the environment and can be used in large patterns must be found or synthesized. Devising an appropriate photocatalyst immobilization strategy to provide a cost-effective solid–liquid separation can save cost and avoid secondary pollution. (iv) A good reactor can improve the utilization rate of light and reduce the electricity costs. Thus, a good design of the reactor is necessary before the experiment. (v) In several cases, toxicity assessment may be even more sensitive than chemical analysis by using modified TiO<sub>2</sub>. (vi) Although modified TiO<sub>2</sub> can have a good degradation effect on pollutants in the laboratory, the durability and recyclability of the catalysts must be considered in actual application.

Facing the problems of complex types of pollutants and tight treatment time, the comprehensive application of multiple treatments for pollutants is the development direction of the current environmental field. The combined use of photocatalysis and other technologies will broaden the application of photocatalysis technology.

**Author Contributions:** R.L. is mainly responsible for the writing of article content and pictures. T.L. modified the article content and pictures. Q.Z. determined the direction of the article. All authors have read and agreed to the published version of the manuscript.

**Funding:** This work was financially supported by National Natural Science Foundation of China (21876090), the Tianjin Research Program of Application Foundation and Advanced Technology (18JCZDJC39400 and 19YFZCSF00920), the Postdoctoral Science Foundation of China (2019M660985) and the 111 program of the Ministry of Education of China (T2017002).

**Acknowledgments:** We acknowledge the use of facilities within the School of Environmental Science and Engineering at Nankai University.

**Conflicts of Interest:** The authors declare no conflict of interest.

## References

1. Fujishima, A.; Honda, K. Electrochemical photolysis of water at a semiconductor electrode. *Nature* **1972**, *238*, 37–38. [[CrossRef](#)]
2. Carey, J.H.; Lawrence, J.; Tosine, H.M. Photodechlorination of PCB's in the presence of titanium dioxide in aqueous suspensions. *Bull. Environ. Contam. Toxicol.* **1976**, *16*, 697–701. [[CrossRef](#)]
3. Frank, S.N.; Bard, A.J. Heterogeneous photocatalytic oxidation of cyanide and sulfite in aqueous solutions at semiconductor powders. *J. Phys. Chem.* **1977**, *81*, 1484–1488. [[CrossRef](#)]
4. Xu, M.X.; Wang, Y.H.; Geng, J.F.; Jing, D.W. Photodecomposition of NO<sub>x</sub> on Ag/TiO<sub>2</sub> composite catalysts in a gas phase reactor. *Chem. Eng. J.* **2017**, *307*, 181–188. [[CrossRef](#)]
5. Karthikeyan, C.; Arunachalam, P.; Ramachandran, K.; Al-Mayouf, A.M.; Karuppuchamy, S. Recent advances in semiconductor metal oxides with enhanced methods for solar photocatalytic applications. *J. Alloys Compd.* **2020**, *828*, 154281. [[CrossRef](#)]
6. Li, Z.Y.; Cao, F.; Wang, L.; Chen, Z.W.; Ji, X.H. A novel ternary MoS<sub>2</sub>/MoO<sub>3</sub>/TiO<sub>2</sub> composite for fast photocatalytic degradation of rhodamine B under visible-light irradiation. *New J. Chem.* **2020**, *44*, 537–542. [[CrossRef](#)]
7. Paeng, D.S.; Huy, B.T.; Phuong, N.T.K.; Dao, V.D.; Lee, Y.I. Photocatalytic activity of Yb, Er, Ce-codoped TiO<sub>2</sub> for degradation of Rhodamine B and 4-chlorophenol. *J. Chem. Technol. Biot.* **2019**. [[CrossRef](#)]
8. Chen, Y.F.; Tang, X.N.; Zhang, B.; Luo, Y.; Li, Y. TiO<sub>2</sub>@SiO<sub>2</sub> Composites: Preparation and Photocatalytic Antimicrobial Performance. *J. Inorg. Mater.* **2019**, *34*, 1325–1333. [[CrossRef](#)]
9. Yang, D.; Zou, X.Y.; Sun, Y.Y.; Tong, Z.W.; Jiang, Z.Y. Fabrication of three-dimensional porous La-doped SrTiO<sub>3</sub> microspheres with enhanced visible light catalytic activity for Cr(VI) reduction. *Front. Chem. Sci. Eng.* **2018**, *12*, 440–449. [[CrossRef](#)]
10. Yu, X.; Lin, Y.; Liu, H.; Yang, C.; Peng, Y.; Du, C.; Wu, S.; Li, X.; Zhong, Y. Photocatalytic performances of heterojunction catalysts of silver phosphate modified by PANI and Cr-doped SrTiO<sub>3</sub> for organic pollutant removal from high salinity wastewater. *J. Colloid Interface Sci.* **2020**, *561*, 379–395. [[CrossRef](#)] [[PubMed](#)]

11. Zhao, Z.H.; Zhang, X.; Lei, Y.Y.; Yang, P.F.; Fan, J.M.; Zhang, B.; Yin, S. Exceptional photocatalytic activity for Ag,Cr- SrTiO<sub>3</sub> activated by H<sub>2</sub>O<sub>2</sub> for removal of organic pollutants. *Mater. Res. Express* **2020**, *7*, 015034. [[CrossRef](#)]
12. Saidani, T.; Zaabat, M.; Aida, M.S.; Boudine, B. Effect of copper doping on the photocatalytic activity of ZnO thin films prepared by sol-gel method. *Superlattices Microstruct.* **2015**, *88*, 315–322. [[CrossRef](#)]
13. Das, A.; Nair, R.G. Effect of aspect ratio on photocatalytic performance of hexagonal ZnO nanorods. *J. Alloys Compd.* **2020**, *817*, 153277. [[CrossRef](#)]
14. Shkir, M.; Al-Shehri, B.M.; Pachamuthu, M.P.; Khan, A.; Chandekar, K.V.; AlFaify, S.; Hamdy, M.S. A remarkable improvement in photocatalytic activity of ZnO nanoparticles through Sr doping synthesized by one pot flash combustion technique for water treatments. *Colloid Surf. A Physicochem. Eng. Asp.* **2020**, *587*, 124340. [[CrossRef](#)]
15. Mena, E.; Rey, A.; Rodriguez, E.M.; Beltran, F.J. Reaction mechanism and kinetics of DEET visible light assisted photocatalytic ozonation with WO<sub>3</sub> catalyst. *Appl. Catal. B* **2017**, *202*, 460–472. [[CrossRef](#)]
16. Zeng, W.G.; Cai, T.; Liu, Y.T.; Wang, L.L.; Dong, W.Y.; Chen, H.; Xia, X.N. An artificial organic-inorganic Z-scheme photocatalyst WO<sub>3</sub>@Cu@PDI supramolecular with excellent visible light absorption and photocatalytic activity. *Chem. Eng. J.* **2020**, *381*, 122691. [[CrossRef](#)]
17. Rosaline, D.R.; Inbanathan, S.S.R.; Suganthi, A.; Rajarajan, M.; Kavitha, G.; Srinivasan, R.; Hegazy, H.H.; Umar, A.; Algarni, H.; Manikandan, E. Visible-Light Driven Photocatalytic Degradation of Eosin Yellow (EY) Dye Based on NiO-WO<sub>3</sub> Nanoparticles. *J. Nanosci. Nanotechnol.* **2020**, *20*, 924–933. [[CrossRef](#)]
18. Gionco, C.; Hernandez, S.; Castellino, M.; Gadhi, T.A.; Munoz-Tabares, J.A.; Cerrato, E.; Tagliaferro, A.; Russo, N.; Paganini, M.C. Synthesis and characterization of Ce and Er doped ZrO<sub>2</sub> nanoparticles as solar light driven photocatalysts. *J. Alloys Compd.* **2019**, *775*, 896–904. [[CrossRef](#)]
19. Al-Namshah, K.S.; Mohamed, R.M. Co<sub>3</sub>O<sub>4</sub>-ZrO<sub>2</sub> nanocomposites: Simple preparation and enhanced photocatalytic performance for cyanide degradation under visible light. *Desalin. Water Treat.* **2019**, *145*, 318–325. [[CrossRef](#)]
20. Reddy, C.V.; Reddy, I.N.; Ravindranadh, K.; Reddy, K.R.; Shetti, N.P.; Kim, D.; Shim, J.; Aminabhavi, T.M. Copper-doped ZrO<sub>2</sub> nanoparticles as high-performance catalysts for efficient removal of toxic organic pollutants and stable solar water oxidation. *J. Environ. Manag.* **2020**, *260*, 110088. [[CrossRef](#)]
21. Nguyen, T.B.; Huang, C.P.; Doong, R.A.; Chen, C.W.; Dong, C.D. Visible-light photodegradation of sulfamethoxazole (SMX) over Ag-P-codoped g-C<sub>3</sub>N<sub>4</sub> (Ag-P@UCN) photocatalyst in water. *Chem. Eng. J.* **2020**, *384*, 123383. [[CrossRef](#)]
22. Zhang, J.J.; Zhu, Z.R.; Jiang, J.C.; Li, H. Fabrication of a novel AgI/LaFeO<sub>3</sub>/g-C<sub>3</sub>N<sub>4</sub> dual Z-scheme photocatalyst with enhanced photocatalytic performance. *Mater. Lett.* **2020**, *262*, 127029. [[CrossRef](#)]
23. Liu, X.M.; Liu, Y.; Zhang, W.K.; Zhong, Q.Y.; Ma, X.Y. In situ self-assembly of 3D hierarchical 2D/2D CdS/g-C<sub>3</sub>N<sub>4</sub> heterojunction with excellent photocatalytic performance. *Mater. Sci. Semicond. Proc.* **2020**, *105*, 104734. [[CrossRef](#)]
24. Nalid, N.R.; Majid, A.; Tahir, M.B.; Niaz, N.A.; Khalid, S. Carbonaceous-TiO<sub>2</sub> nanomaterials for photocatalytic degradation of pollutants: A review. *Ceram. Int.* **2017**, *43*, 14552–14571.
25. Hafeez, H.Y.; Lakhera, S.K.; Karthik, P.; Anpo, M.; Neppolian, B. Facile construction of ternary CuFe<sub>2</sub>O<sub>4</sub>-TiO<sub>2</sub> nanocomposite supported reduced graphene oxide (rGO) photocatalysts for the efficient hydrogen production. *Appl. Surf. Sci.* **2018**, *449*, 772–779. [[CrossRef](#)]
26. Khedr, T.M.; El-Sheikh, S.M.; Ismail, A.A.; Kowalska, E.; Bahnemann, D.W. Photodegradation of Microcystin-LR Using Visible Light-Activated C/N-co-Modified Mesoporous TiO<sub>2</sub> Photocatalyst. *Materials* **2019**, *12*, 1027. [[CrossRef](#)] [[PubMed](#)]
27. Zhang, S.C.; Lu, X.J. Treatment of wastewater containing Reactive Brilliant Blue KN-R using TiO<sub>2</sub>/BC composite as heterogeneous photocatalyst and adsorbent. *Chemosphere* **2018**, *206*, 777–783. [[CrossRef](#)]
28. Li, Y.K.; Zhang, P.; Wan, D.Y.; Xue, C.; Zhao, J.T.; Shao, G.S. Direct evidence of 2D/1D heterojunction enhancement on photocatalytic activity through assembling MoS<sub>2</sub> nanosheets onto super-long TiO<sub>2</sub> nanofibers. *Appl. Surf. Sci.* **2020**, *504*, 144361. [[CrossRef](#)]
29. Pelaez, M.; Nolan, N.T.; Pillai, S.C.; Seery, M.K.; Falaras, P.; Kontos, A.G.; Dunlop, P.S.M.; Hamilton, J.W.J.; Byrne, J.A.; O'Shea, K.; et al. A review on the visible light active titanium dioxide photocatalysts for environmental applications. *Appl. Catal. B Environ.* **2012**, *125*, 331–349. [[CrossRef](#)]

30. Liu, W.; Zhao, X.; Borthwick, A.G.L.; Wang, Y.Q.; Ni, J.R. Dual-Enhanced Photocatalytic Activity of Fe-Deposited Titanate Nanotubes Used for Simultaneous Removal of As(III) and As(V). *ACS Appl. Mater. Interfaces* **2015**, *7*, 19726–19735. [[CrossRef](#)]
31. Cai, Z.; Zhao, X.; Wang, T.; Liu, W.; Zhao, D. Reusable Platinum-Deposited Anatase/Hexa-Titanate Nanotubes: Roles of Reduced and Oxidized Platinum on Enhanced Solar-Light-Driven Photocatalytic Activity. *ACS Sustain. Chem. Eng.* **2017**, *5*, 547–555. [[CrossRef](#)]
32. Shankar, R.; Shim, W.J.; An, J.G.; Yim, U.H. A practical review on photooxidation of crude oil: Laboratory lamp setup and factors affecting it. *Water Res.* **2015**, *68*, 304–315. [[CrossRef](#)] [[PubMed](#)]
33. Tian, J.; Zhao, Z.H.; Kumar, A.; Boughton, R.I.; Liu, H. Recent progress in design, synthesis, and applications of one-dimensional TiO<sub>2</sub> nanostructured surface heterostructures: A review. *Chem. Soc. Rev.* **2014**, *43*, 6920–6937. [[CrossRef](#)] [[PubMed](#)]
34. Dahl, M.; Liu, Y.; Yin, Y. Composite Titanium Dioxide Nanomaterials. *Chem. Rev.* **2014**, *114*, 9853–9889. [[CrossRef](#)]
35. Hlekelele, L.; Durbach, S.H.; Chauke, V.P.; Dziike, F.; Franklyn, P.J. Resin-gel incorporation of high concentrations of W<sup>6+</sup> and Zn<sup>2+</sup> into TiO<sub>2</sub>-anatase crystal to form quaternary mixed-metal oxides: Effect on the a lattice parameter and photodegradation efficiency. *RSC Adv.* **2019**, *9*, 36875–36883. [[CrossRef](#)]
36. Nzaba, S.K.M.; Nyoni, H.H.; Mamba, B.B.; Kuvarega, A.T. Comparative Study of Dendrimer-Templated Nitrogen-Platinum Co-Doped TiO<sub>2</sub> for the Photocatalytic Degradation of Azo Dyes in Contaminated Water. *Chemistryselect* **2019**, *4*, 12156–12163. [[CrossRef](#)]
37. Sun, D.W.; Li, Y.J.; Cao, T.P.; Zhao, Y.H.; Yang, D.K. Preparation of Dy<sub>3+</sub>-doped YVO<sub>4</sub>/TiO<sub>2</sub> Composite Nanofibers with Three-dimensional Net-like Structure and Enhanced Photocatalytic Activity for Hydrogen Evolution. *Chem. J. Chin. Univ. Chin.* **2019**, *40*, 2348–2353. [[CrossRef](#)]
38. Deng, H.Y.; He, H.; Sun, S.J.; Zhu, X.T.; Zhou, D.X.; Han, F.X.; Huang, B.; Pan, X.J. Photocatalytic degradation of dye by Ag/TiO<sub>2</sub> nanoparticles prepared with different sol-gel crystallization in the presence of effluent organic matter. *Environ. Sci. Pollut. Res.* **2019**, *26*, 35900–35912. [[CrossRef](#)] [[PubMed](#)]
39. Yoshida, T.; Misu, Y.; Yamamoto, M.; Tanabe, T.; Kumagai, J.; Ogawa, S.; Yagi, S. Effects of the amount of Au nanoparticles on the visible light response of TiO<sub>2</sub> photocatalysts. *Catal. Today* **2020**, *352*, 34–38. [[CrossRef](#)]
40. Yang, L.X.; Chen, Z.; Zhang, J.; Wang, C.A. SrTiO<sub>3</sub>/TiO<sub>2</sub> heterostructure nanowires with enhanced electron-hole separation for efficient photocatalytic activity. *Front. Mater. Sci.* **2019**, *13*, 342–351. [[CrossRef](#)]
41. Al Jitan, S.; Palmisano, G.; Garlisi, C. Synthesis and Surface Modification of TiO<sub>2</sub>-Based Photocatalysts for the Conversion of CO<sub>2</sub>. *Catalysts* **2020**, *10*, 227. [[CrossRef](#)]
42. Serpone, N. Is the band gap of pristine TiO<sub>2</sub> narrowed by anion- and cation-doping of titanium dioxide in second-generation photocatalysts? *J. Phys. Chem. B* **2006**, *110*, 24287–24293. [[CrossRef](#)]
43. Devi, L.G.; Kavitha, R. A review on non metal ion doped titania for the photocatalytic degradation of organic pollutants under UV/solar light: Role of photogenerated charge carrier dynamics in enhancing the activity. *Appl. Catal. B Environ.* **2013**, *140*, 559–587. [[CrossRef](#)]
44. Asahi, R.; Morikawa, T.; Irie, H.; Ohwaki, T. Nitrogen-Doped Titanium Dioxide as Visible-Light-Sensitive Photocatalyst: Designs, Developments, and Prospects. *Chem. Rev.* **2014**, *114*, 9824–9852. [[CrossRef](#)] [[PubMed](#)]
45. Liao, F.; Chu, L.F.; Guo, C.X.; Guo, Y.J.; Ke, Q.F.; Guo, Y.P. Ytterbium Doped TiO<sub>2</sub> Nanofibers on Activated Carbon Fibers Enhances Adsorption and Photocatalytic Activities for Toluene Removal. *Chemistryselect* **2019**, *4*, 9222–9231. [[CrossRef](#)]
46. Suarez, S.; Jansson, I.; Ohtani, B.; Sanchez, B. From titania nanoparticles to decahedral anatase particles: Photocatalytic activity of TiO<sub>2</sub>/zeolite hybrids for VOCs oxidation. *Catal. Today* **2019**, *326*, 2–7. [[CrossRef](#)]
47. Liang, H.; Wang, Z.Q.; Liao, L.M.; Chen, L.; Li, Z.; Feng, J. High performance photocatalysts: Montmorillonite supported-nano TiO<sub>2</sub> composites. *Optik* **2017**, *136*, 44–51. [[CrossRef](#)]
48. Zhu, P.F.; Ren, Z.H.; Wang, R.X.; Duan, M.; Xie, L.S.; Xu, J.; Tian, Y.J. Preparation and visible photocatalytic dye degradation of Mn-TiO<sub>2</sub>/sepiolite photocatalysts. *Front. Mater. Sci.* **2020**, *14*, 33–42. [[CrossRef](#)]
49. Saqib, N.U.; Adnan, R.; Shah, I. Zeolite supported TiO<sub>2</sub> with enhanced degradation efficiency for organic dye under household compact fluorescent light. *Mater. Res. Express* **2019**, *6*, 095506. [[CrossRef](#)]
50. Malakootian, M.; Nasiri, A.; Gharaghani, M.A. Photocatalytic degradation of ciprofloxacin antibiotic by TiO<sub>2</sub> nanoparticles immobilized on a glass plate. *Chem. Eng. Commun.* **2020**, *207*, 56–72. [[CrossRef](#)]

51. Espino-Estevez, M.R.; Fernandez-Rodriguez, C.; Gonzalez-Diaz, O.M.; Navio, J.A.; Fernandez-Hevia, D.; Dona-Rodriguez, J.M. Enhancement of stability and photoactivity of TiO<sub>2</sub> coatings on annular glass reactors to remove emerging pollutants from waters. *Chem. Eng. J.* **2015**, *279*, 488–497. [[CrossRef](#)]
52. Pierpaoli, M.; Lewkowicz, A.; Rycewi'cz, M.; Szczodrowski, K.; Ruello, M.L.; Bogdanowicz, R. Enhanced photocatalytic activity of transparent carbon nanowall/TiO<sub>2</sub> heterostructures. *Mater. Lett.* **2020**, *262*, 127155. [[CrossRef](#)]
53. Chu, Z.D.; Qiu, L.L.; Chen, Y.; Zhuang, Z.S.; Du, P.F.; Xiong, J. TiO<sub>2</sub>-loaded carbon fiber: Microwave hydrothermal synthesis and photocatalytic activity under UV light irradiation. *J. Phys. Chem. Solids* **2020**, *136*, 109138. [[CrossRef](#)]
54. Hu, C.Y.; Lei, E.; Hu, K.K.; Lai, L.Y.; Zhao, D.; Zhao, W.; Rong, H. Simple synthesis of 3D flower-like g-C<sub>3</sub>N<sub>4</sub>/TiO<sub>2</sub> composite microspheres for enhanced visible-light photocatalytic activity. *J. Mater. Sci.* **2020**, *55*, 151–162. [[CrossRef](#)]
55. Cunha, D.L.; Kuznetsov, A.; Araujo, J.R.; Neves, R.S.; Archanjo, B.S.; Canela, M.C.; Marques, M. Optimization of Benzodiazepine Drugs Removal from Water by Heterogeneous Photocatalysis Using TiO<sub>2</sub>/Activated Carbon Composite. *Water Air Soil Pollut.* **2019**, *230*, 141. [[CrossRef](#)]
56. Zhang, Y.Y.; Jiang, Z.L.; Huang, J.Y.; Lim, L.Y.; Li, W.L.; Deng, J.Y.; Gong, D.G.; Tang, Y.X.; Lai, Y.K.; Chen, Z. Titanate and titania nanostructured materials for environmental and energy applications: A review. *RSC Adv.* **2015**, *5*, 79479–79510. [[CrossRef](#)]
57. Zhao, X.; Cai, Z.Q.; Wang, T.; O'Reilly, S.E.; Liu, W.; Zhao, D.Y. A new type of cobalt-deposited titanate nanotubes for enhanced photocatalytic degradation of phenanthrene. *Appl. Catal. B Environ.* **2016**, *187*, 134–143. [[CrossRef](#)]
58. Doong, R.-A.; Liao, C.-Y. Enhanced visible-light-responsive photodegradation of bisphenol A by Cu, N-codoped titanate nanotubes prepared by microwave-assisted hydrothermal method. *J. Hazard. Mater.* **2017**, *322*, 254–262. [[CrossRef](#)] [[PubMed](#)]
59. Liu, W.; Sun, W.L.; Borthwick, A.G.L.; Wang, T.; Li, F.; Guan, Y.D. Simultaneous removal of Cr(VI) and 4-chlorophenol through photocatalysis by a novel anatase/titanate nanosheet composite: Synergetic promotion effect and autosynchronous doping. *J. Hazard. Mater.* **2016**, *317*, 385–393. [[CrossRef](#)]
60. Zhao, X.; Du, P.H.; Cai, Z.Q.; Wang, T.; Fu, J.; Liu, W. Photocatalysis of bisphenol A by an easy-settling titania/titanate composite: Effects of water chemistry factors, degradation pathway and theoretical calculation. *Environ. Pollut.* **2018**, *232*, 580–590. [[CrossRef](#)]
61. Li, F.; Du, P.H.; Liu, W.; Li, X.S.; Ji, H.D.; Duan, J.; Zhao, D.Y. Hydrothermal synthesis of graphene grafted titania/titanate nanosheets for photocatalytic degradation of 4-chlorophenol: Solar-light-driven photocatalytic activity and computational chemistry analysis. *Chem. Eng. J.* **2018**, *331*, 685–694. [[CrossRef](#)]
62. Cheng, K.Y.; Cai, Z.Q.; Fu, J.; Sun, X.B.; Sun, W.L.; Chen, L.; Zhang, D.D.; Liu, W. Synergistic adsorption of Cu(II) and photocatalytic degradation of phenanthrene by a jaboticaba-like TiO<sub>2</sub>/titanate nanotube composite: An experimental and theoretical study. *Chem. Eng. J.* **2019**, *358*, 1155–1165. [[CrossRef](#)]
63. Ji, H.D.; Du, P.H.; Zhao, D.Y.; Li, S.; Sun, F.B.; Duin, E.C.; Liu, W. 2D/1D graphitic carbon nitride/titanate nanotubes heterostructure for efficient photocatalysis of sulfamethazine under solar light: Catalytic “hot spots” at the rutile-anatase-titanate interfaces. *Appl. Catal. B* **2020**, *263*, 118357. [[CrossRef](#)]
64. Tu, H.; Li, D.; Yi, Y.; Liu, R.; Wu, Y.; Dong, X.Y.; Shi, X.W.; Deng, H.B. Incorporation of rectorite into porous polycaprolactone/TiO<sub>2</sub> nanofibrous mats for enhancing photocatalysis properties towards organic dye pollution. *Compos. Commun.* **2019**, *15*, 58–63. [[CrossRef](#)]
65. Ni, Y.H.; Yan, K.; Xu, F.Y.; Zhong, W.B.; Zhao, Q.H.; Liu, K.; Yan, K.L.; Wang, D. Synergistic effect on TiO<sub>2</sub> doped poly (vinyl alcohol-co-ethylene) nanofibrous film for filtration and photocatalytic degradation of methylene blue. *Compos. Commun.* **2019**, *12*, 112–116. [[CrossRef](#)]
66. Mohsenzadeh, M.; Mirbagheri, S.A.; Sabbaghi, S. Photocatalytic degradation of 1,2-dichloroethane using immobilized PANI-TiO<sub>2</sub> nanocomposite in a pilot-scale packed bed reactor. *Desalin. Water Treat.* **2019**, *155*, 72–83. [[CrossRef](#)]
67. Qin, Y.Y.; Li, H.; Lu, J.; Meng, F.Y.; Ma, C.C.; Yan, Y.S.; Meng, M.J. Nitrogen-doped hydrogenated TiO<sub>2</sub> modified with CdS nanorods with enhanced optical absorption, charge separation and photocatalytic hydrogen evolution. *Chem. Eng. J.* **2020**, *384*, 123275. [[CrossRef](#)]
68. Ratova, M.; West, G.T.; Kelly, P.J.; Xia, X.; Gao, Y. Synergistic effect of doping with nitrogen and molybdenum on the photocatalytic properties of thin titania films. *Vacuum* **2015**, *114*, 205–212. [[CrossRef](#)]

69. Kovalevskiy, N.; Selishchev, D.; Svintsitskiy, D.; Selishcheva, S.; Berezin, A.; Kozlov, D. Synergistic effect of polychromatic radiation on visible light activity of N-doped TiO<sub>2</sub> photocatalyst. *Catal. Commun.* **2020**, *134*, 105841. [[CrossRef](#)]
70. Fang, W.Z.; Xing, M.Y.; Zhang, J.L. Modifications on reduced titanium dioxide photocatalysts: A review. *J. Photochem. Photobiol. C* **2017**, *32*, 21–39. [[CrossRef](#)]
71. Reda, S.M.; Khairy, M.; Mousa, M.A. Photocatalytic activity of nitrogen and copper doped TiO<sub>2</sub> nanoparticles prepared by microwave-assisted sol-gel process. *Arab. J. Chem.* **2020**, *13*, 86–95. [[CrossRef](#)]
72. Jin, X.D.; Zhou, X.Q.; Sun, P.; Lin, S.Y.; Cao, W.B.; Li, Z.F.; Liu, W.X. Photocatalytic degradation of norfloxacin using N-doped TiO<sub>2</sub>: Optimization, mechanism, identification of intermediates and toxicity evaluation. *Chemosphere* **2019**, *237*, 124433. [[CrossRef](#)] [[PubMed](#)]
73. Ji, L.J.; Zhou, S.; Liu, X.; Gong, M.D.; Xu, T. Synthesis of carbon- and nitrogen-doped TiO<sub>2</sub>/carbon composite fibers by a surface-hydrolyzed PAN fiber and their photocatalytic property. *J. Mater. Sci.* **2020**, *55*, 2471–2481. [[CrossRef](#)]
74. Asahi, R.; Morikawa, T.; Ohwaki, T.; Aoki, K.; Taga, Y. Visible-light photocatalysis in nitrogen-doped titanium oxides. *Science* **2001**, *293*, 269–271. [[CrossRef](#)]
75. Li, H.; Hao, Y.B.; Lu, H.Q.; Liang, L.P.; Wang, Y.Y.; Qiu, J.H.; Shi, X.C.; Wang, Y.; Yao, J.F. systematic study on visible-light N-doped TiO<sub>2</sub> photocatalyst obtained from ethylenediamine by sol-gel method. *Appl. Surf. Sci.* **2015**, *344*, 112–118. [[CrossRef](#)]
76. Jyothi, M.S.; Laveena, P.D.; Shwetharani, R.; Balakrishna, G.R. Novel hydrothermal method for effective doping of N and F into nano Titania for both, energy and environmental applications. *Mater. Res. Bull.* **2016**, *74*, 478–484. [[CrossRef](#)]
77. Rahbar, M.; Mehrzad, M.; Behpour, M.; Mohammadi-Aghdam, S.; Ashrafi, M. S, N co-doped carbon quantum dots/TiO<sub>2</sub> nanocomposite as highly efficient visible light photocatalyst. *Nanotechnology* **2019**, *30*, 505702. [[CrossRef](#)]
78. Liu, D.; Wang, J.Q.; Zhou, J.; Xi, Q.H.; Li, X.; Nie, E.; Piao, X.Q.; Sun, Z. Fabricating I doped TiO<sub>2</sub> photoelectrode for the degradation of diclofenac: Performance and mechanism study. *Chem. Eng. J.* **2019**, *369*, 968–978. [[CrossRef](#)]
79. Ichihara, F.; Sieland, F.; Pang, H.; Philo, D.; Duong, A.T.; Chang, K.; Kako, T.; Bahnemann, D.W.; Ye, J.H. Photogenerated Charge Carriers Dynamics on La- and/or Cr-Doped SrTiO<sub>3</sub> Nanoparticles Studied by Transient Absorption Spectroscopy. *J. Phys. Chem. C* **2020**, *124*, 1292–1302. [[CrossRef](#)]
80. Tian, L.J.; Xing, L.; Shen, X.L.; Li, Q.H.; Ge, S.J.; Liu, B.K.; Jie, L. Visible light enhanced Fe-I-TiO<sub>2</sub> photocatalysts for the degradation of gaseous benzene. *Atmos. Pollut. Res.* **2020**, *11*, 179–185. [[CrossRef](#)]
81. Razali, M.H.; Noor, A.F.M.; Yusoff, M. Physicochemical Properties of a Highly Efficient Cu-Ion-Doped TiO<sub>2</sub> Nanotube Photocatalyst for the Degradation of Methyl Orange Under Sunlight. *J. Nanosci. Nanotechnol.* **2020**, *20*, 965–972. [[CrossRef](#)] [[PubMed](#)]
82. Li, Z.; Tian, B.; Zhen, W.L.; Wu, Y.Q.; Lu, G.X. Inhibition of hydrogen and oxygen recombination using oxygen transfer reagent hemin chloride in Pt/TiO<sub>2</sub> dispersion for photocatalytic hydrogen generation. *Appl. Catal. B* **2017**, *203*, 408–415. [[CrossRef](#)]
83. Yu, Y.Q.; Zhu, X.R.; Wang, L.R.; Wu, F.S.; Liu, S.L.; Chang, C.Y.; Luo, X.G. A simple strategy to design 3-layered Au-TiO<sub>2</sub> dual nanoparticles immobilized cellulose membranes with enhanced photocatalytic activity. *Carbohydr. Polym.* **2020**, *231*, 115694. [[CrossRef](#)] [[PubMed](#)]
84. Surya, C.; John, N.A.A.; Pandiyan, V.; Ravikumar, S.; Amutha, P.; Sobral, A.J.F.N.; Krishnakumar, B. Costus speciosus leaf extract assisted CS-Pt-TiO<sub>2</sub> composites: Synthesis, characterization and their bio and photocatalytic applications. *J. Mol. Struct.* **2019**, *1195*, 787–795. [[CrossRef](#)]
85. Maarisetty, D.; Baral, S.S. Defect-induced enhanced dissociative adsorption, optoelectronic properties and interfacial contact in Ce doped TiO<sub>2</sub>: Solar photocatalytic degradation of Rhodamine B. *Ceram Int.* **2019**, *45*, 22253–22263. [[CrossRef](#)]
86. Zhao, J.; Chen, X.Y.; Zhou, Y.H.; Tian, H.J.; Guo, Q.J.; Hu, X.D. Efficient removal of oil pollutant via simultaneous adsorption and photocatalysis using La-N-TiO<sub>2</sub>-cellulose/SiO<sub>2</sub> difunctional aerogel composite. *Res. Chem. Intermed.* **2020**, *46*, 1805–1822. [[CrossRef](#)]
87. Liang, J.C.; Wang, J.Y.; Song, K.X.; Wang, X.F.; Yu, K.F.; Liang, C. Enhanced photocatalytic activities of Nd-doped TiO<sub>2</sub> under visible light using a facile sol-gel method. *J. Rare Earth* **2020**, *38*, 148–156. [[CrossRef](#)]

88. Hu, Z.; Yang, C.; Lv, K.; Li, X.; Li, Q.; Fan, J. Single atomic Au induced dramatic promotion of the photocatalytic activity of TiO<sub>2</sub> hollow microspheres. *Chem. Commun. Camb. Engl.* **2020**, *56*, 1745–1748. [[CrossRef](#)]
89. Hayashi, T.; Nakamura, K.; Suzuki, T.; Saito, N.; Murakami, Y. OH radical formation by the photocatalytic reduction reactions of H<sub>2</sub>O<sub>2</sub> on the surface of plasmonic excited Au-TiO<sub>2</sub> photocatalysts. *Chem. Phys. Lett.* **2020**, *739*, 136958. [[CrossRef](#)]
90. Jeantelot, G.; Qureshi, M.; Harb, M.; Ould-Chikh, S.; Anjum, D.H.; Abou-Hamad, E.; Aguilar-Tapia, A.; Hazemann, J.L.; Takanabe, K.; Basset, J.M. TiO<sub>2</sub>-supported Pt single atoms by surface organometallic chemistry for photocatalytic hydrogen evolution. *Phys. Chem. Chem. Phys.* **2019**, *21*, 24429–24440. [[CrossRef](#)]
91. Singhal, N.; Kumar, U. Noble metal modified TiO<sub>2</sub>: Selective photoreduction of CO<sub>2</sub> to hydrocarbons. *Mol. Catal.* **2017**, *439*, 91–99. [[CrossRef](#)]
92. Gao, P.; Yang, L.B.; Xiao, S.T.; Wang, L.Y.; Guo, W.; Lu, J.H. Effect of Ru, Rh, Mo, and Pd Adsorption on the Electronic and Optical Properties of Anatase TiO<sub>2</sub>(101): A DFT Investigation. *Materials* **2019**, *12*, 814. [[CrossRef](#)] [[PubMed](#)]
93. Liu, Y.; Xiao, Z.Z.; Cao, S.; Li, J.H.; Piao, L.Y. Controllable synthesis of Au-TiO<sub>2</sub> nanodumbbell photocatalysts with spatial redox region. *Chin. J. Catal.* **2020**, *41*, 219–226. [[CrossRef](#)]
94. Khatun, F.; Abd Aziz, A.; Sim, L.C.; Monir, M.U. Plasmonic enhanced Au decorated TiO<sub>2</sub> nanotube arrays as a visible light active catalyst towards photocatalytic CO<sub>2</sub> conversion to CH<sub>4</sub>. *J. Environ. Chem. Eng.* **2019**, *7*. [[CrossRef](#)]
95. Sacco, O.; Murcia, J.J.; Lara, A.E.; Hernandez-Laverde, M.; Rojas, H.; Navio, J.A.; Hidalgo, M.C.; Vaiano, V. Pt-TiO<sub>2</sub>-Nb<sub>2</sub>O<sub>5</sub> heterojunction as effective photocatalyst for the degradation of diclofenac and ketoprofen. *Mater. Sci. Semicond. Proc.* **2020**, *107*, 104839. [[CrossRef](#)]
96. Qu, J.F.; Chen, D.Y.; Li, N.J.; Xu, Q.F.; Li, H.; He, J.H.; Lu, J.M. Ternary photocatalyst of atomic-scale Pt coupled with MoS<sub>2</sub> co-loaded on TiO<sub>2</sub> surface for highly efficient degradation of gaseous toluene. *Appl. Catal. B* **2019**, *256*. [[CrossRef](#)]
97. Ouyang, W.Y.; Munoz-Batista, M.J.; Kubacka, A.; Luque, R.; Fernandez-Garcia, M. Enhancing photocatalytic performance of TiO<sub>2</sub> in H<sub>2</sub> evolution via Ru co-catalyst deposition. *Appl. Catal B Environ.* **2018**, *238*, 434–443. [[CrossRef](#)]
98. Li, F.; Huang, H.B.; Li, G.S.; Leung, D.Y.C. TiO<sub>2</sub> nanotube arrays modified with nanoparticles of platinum group metals (Pt, Pd, Ru): Enhancement on photoelectrochemical performance. *J. Nanopart Res.* **2019**, *21*, 29. [[CrossRef](#)]
99. Sato, S.; White, J.M. Photodecomposition of water over Pt/TiO<sub>2</sub> catalysts. *Chem. Phys. Lett.* **1980**, *72*, 83–86. [[CrossRef](#)]
100. Kennedy, J.C.; Dartye, A.K. Photothermal heterogeneous oxidation of ethanol over Pt/TiO<sub>2</sub>. *J. Catal.* **1998**, *179*, 375–389. [[CrossRef](#)]
101. Ji, L.J.; Qin, X.; Zheng, J.J.; Zhou, S.; Xu, T.; Shi, G.J. Synthesis of Ag-Carbon-TiO<sub>2</sub> composite tubes and their antibacterial and organic degradation properties. *J. Sol Gel Sci. Technol.* **2020**, *93*, 291–301. [[CrossRef](#)]
102. Shan, R.; Lu, L.L.; Gu, J.; Zhang, Y.Y.; Yuan, H.R.; Chen, Y.; Luo, B. Photocatalytic degradation of methyl orange by Ag/TiO<sub>2</sub>/biochar composite catalysts in aqueous solutions. *Mater. Sci. Semicond. Process.* **2020**, *114*, 105088. [[CrossRef](#)]
103. Jaafar, F.; Jalil, A.A.; Triwahyono, S.; Efendi, J.; Mukti, R.R.; Jusoh, R.; Jusoh, N.W.C.; Karim, A.H.; Salleh, N.F.M.; Suendo, V. Direct in situ activation of Ag<sup>0</sup> nanoparticles in synthesis of Ag/TiO<sub>2</sub> and its photoactivity. *Appl. Surf. Sci.* **2015**, *338*, 75–84. [[CrossRef](#)]
104. Zhu, D.H.; Long, L.; Sun, J.Y.; Wan, H.Q.; Zheng, S.R. Highly active and selective catalytic hydrogenation of p-chloronitrobenzene to p-chloroaniline on Pt@Cu/TiO<sub>2</sub>. *Appl. Surf. Sci.* **2020**, *504*, 144329. [[CrossRef](#)]
105. Nyankson, E.; Agyei-Tuffour, B.; Adjasoo, J.; Ebenezer, A.; Dodoo-Arhin, D.; Yaya, A.; Mensah, B.; Efavi, J.K. Synthesis and Application of Fe-Doped TiO<sub>2</sub>-Halloysite Nanotubes Composite and Their Potential Application in Water Treatment. *Adv. Mater. Sci. Eng.* **2019**, *2019*, 4270310. [[CrossRef](#)]
106. Komaraiah, D.; Radha, E.; Sivakumar, J.; Reddy, M.V.R.; Sayanna, R. Structural, optical properties and photocatalytic activity of Fe<sup>3+</sup> doped TiO<sub>2</sub> thin films deposited by sol-gel spin coating. *Surf. Interfaces* **2019**, *17*, 100368. [[CrossRef](#)]
107. Bhardwaj, S.; Dogra, D.; Pal, B.; Singh, S. Photodeposition time dependant growth, size and photoactivity of Ag and Cu deposited TiO<sub>2</sub> nanocatalyst under solar irradiation. *Sol. Energy* **2019**, *194*, 618–627. [[CrossRef](#)]

108. Ghanbari, S.; Givianrad, M.H.; Azar, P.A. Synthesis and characterization of visible light driven N-Fe-codoped TiO<sub>2</sub>/SiO<sub>2</sub> for simultaneous photoremoval of Cr (VI) and azo dyes in a novel fixed bed continuous flow photoreactor. *Can. J. Chem. Eng.* **2020**, *98*, 705–716. [[CrossRef](#)]
109. Ahadi, S.; Moalej, N.S.; Sheibani, S. Characteristics and photocatalytic behavior of Fe and Cu doped TiO<sub>2</sub> prepared by combined sol-gel and mechanical alloying. *Solid State Sci.* **2019**, *96*, 105975. [[CrossRef](#)]
110. Zhang, J.H.; Fu, D.; Wang, S.Q.; Hao, R.L.; Xie, Y.X. Photocatalytic removal of chromium(VI) and sulfite using transition metal (Cu, Fe, Zn) doped TiO<sub>2</sub> driven by visible light: Feasibility, mechanism and kinetics. *J. Ind. Eng. Chem.* **2019**, *80*, 23–32. [[CrossRef](#)]
111. Khan, M.A.M.; Siwach, R.; Kumar, S.; Alhazaa, A.N. Role of Fe doping in tuning photocatalytic and photoelectrochemical properties of TiO<sub>2</sub> for photodegradation of methylene blue. *Opt. Laser Technol.* **2019**, *118*, 170–178. [[CrossRef](#)]
112. Bhatia, V.; Dhir, A. Transition metal doped TiO<sub>2</sub> mediated photocatalytic degradation of anti-inflammatory drug under solar irradiations. *J. Environ. Chem. Eng.* **2016**, *4*, 1267–1273. [[CrossRef](#)]
113. Stucchi, M.; Boffito, D.C.; Pargoletti, E.; Cerrato, G.; Bianchi, C.L.; Cappelletti, G. Nano-MnO<sub>2</sub> Decoration of TiO<sub>2</sub> Microparticles to Promote Gaseous Ethanol Visible Photoremoval. *Nanomaterials* **2018**, *8*, 686. [[CrossRef](#)]
114. Choi, W.; Termin, A.; Hoffmann, M.R. The Role of Metal Ion Dopants in Quantum-Sized TiO<sub>2</sub>: Correlation between Photoreactivity and Charge Carrier Recombination Dynamics. *J. Phys. Chem.* **1994**, *98*, 13669–13679. [[CrossRef](#)]
115. Du, X.-Q.; Ma, X.-L.; Wang, Y.-J.; Gu, F.-N.; Zhang, J. Optimization of the Ge/TiO<sub>2</sub> catalyst for the degradation of ciprofloxacin by the response surface methodology. *Zhongguo Kangshengsu Zazhi* **2019**, *44*, 750–757.
116. Crisan, M.; Mardare, D.; Ianculescu, A.; Dragan, N.; Nitoi, I.; Crisan, D.; Voicescu, M.; Todan, L.; Oancea, P.; Adomnitei, C.; et al. Iron doped TiO<sub>2</sub> films and their photoactivity in nitrobenzene removal from water. *Appl. Surf. Sci.* **2018**, *455*, 201–215. [[CrossRef](#)]
117. Gnanasekaran, L.; Hemamalini, R.; Saravanan, R.; Ravichandran, K.; Gracia, F.; Gupta, V.K. Intermediate state created by dopant ions (Mn, Co and Zr) into TiO<sub>2</sub> nanoparticles for degradation of dyes under visible light. *J. Mol. Liq.* **2016**, *223*, 652–659. [[CrossRef](#)]
118. Huang, J.G.; Guo, X.T.; Wang, B.; Li, L.Y.; Zhao, M.X.; Dong, L.L.; Liu, X.J.; Huang, Y.T. Synthesis and Photocatalytic Activity of Mo-Doped TiO<sub>2</sub> Nanoparticles. *J. Spectrosc.* **2015**, *2015*, 681850. [[CrossRef](#)]
119. Wang, Q.; Jin, R.; Zhang, M.; Gao, S. Solvothermal preparation of Fe-doped TiO<sub>2</sub> nanotube arrays for enhancement in visible light induced photoelectrochemical performance. *J. Alloys Compd.* **2017**, *690*, 139–144. [[CrossRef](#)]
120. Vinodgopal, K.; Kamat, P.V. Enhanced Rates of Photocatalytic Degradation of an Azo Dye Using SnO<sub>2</sub>/TiO<sub>2</sub> Coupled Semiconductor Thin Films. *Environ. Sci. Technol.* **1995**, *29*, 841–845. [[CrossRef](#)]
121. Low, J.; Yu, J.; Jaroniec, M.; Wageh, S.; Al-Ghamdi, A.A. Heterojunction Photocatalysts. *Adv. Mater.* **2017**, *29*, 1601694. [[CrossRef](#)] [[PubMed](#)]
122. Kaur, P.K.; Badru, R.; Singh, P.P.; Kaushal, S. Photodegradation of organic pollutants using heterojunctions: A review. *J. Environ. Chem. Eng.* **2020**, *8*, 103666. [[CrossRef](#)]
123. Li, H.J.; Zhou, Y.; Tu, W.G.; Ye, J.H.; Zou, Z.G. State-of-the-Art Progress in Diverse Heterostructured Photocatalysts toward Promoting Photocatalytic Performance. *Adv. Funct. Mater.* **2015**, *25*, 998–1013. [[CrossRef](#)]
124. Dursun, S.; Kaya, I.C.; Kalem, V.; Akyildiz, H. UV/visible light active CuCrO<sub>2</sub> nanoparticle-SnO<sub>2</sub> nanofiber p-n heterostructured photocatalysts for photocatalytic applications. *Dalton Trans.* **2018**, *47*, 14662–14678. [[CrossRef](#)] [[PubMed](#)]
125. Zhang, W.P.; Xiao, X.Y.; Li, Y.; Zeng, X.Y.; Zheng, L.L.; Wan, C.X. Liquid-exfoliation of layered MoS<sub>2</sub> for enhancing photocatalytic activity of TiO<sub>2</sub>/g-C<sub>3</sub>N<sub>4</sub> photocatalyst and DFT study. *Appl. Surf. Sci.* **2016**, *389*, 496–506. [[CrossRef](#)]
126. Yang, L.; Gao, M.G.; Dai, B.; Guo, X.H.; Liu, Z.Y.; Peng, B.H. Synthesis of spindle-shaped AgI/TiO<sub>2</sub> nanoparticles with enhanced photocatalytic performance. *Appl. Surf. Sci.* **2016**, *386*, 337–344. [[CrossRef](#)]
127. Demirci, S.; Dikici, T.; Yurddaskal, M.; Gultekin, S.; Toparli, M.; Celik, E. Synthesis and characterization of Ag doped TiO<sub>2</sub> heterojunction films and their photocatalytic performances. *Appl. Surf. Sci.* **2016**, *390*, 591–601. [[CrossRef](#)]

128. Sarkar, A.; Gracia-Espino, E.; Wagberg, T.; Shchukarev, A.; Mohl, M.; Rautio, A.R.; Pitkanen, O.; Sharifi, T.; Kordas, K.; Mikkola, J.P. Photocatalytic reduction of CO<sub>2</sub> with H<sub>2</sub>O over modified TiO<sub>2</sub> nanofibers: Understanding the reduction pathway. *Nano Res.* **2016**, *9*, 1956–1968. [[CrossRef](#)]
129. Low, J.X.; Cheng, B.; Yu, J.G. Surface modification and enhanced photocatalytic CO<sub>2</sub> reduction performance of TiO<sub>2</sub>: A review. *Appl. Surf. Sci.* **2017**, *392*, 658–686. [[CrossRef](#)]
130. Moniz, S.J.A.; Shevlin, S.A.; Martin, D.J.; Guo, Z.X.; Tang, J.W. Visible-light driven heterojunction photocatalysts for water splitting—A critical review. *Energy Environ. Sci.* **2015**, *8*, 731–759. [[CrossRef](#)]
131. Kumar, A.; Khan, M.; He, J.H.; Lo, I.M.C. Recent developments and challenges in practical application of visible-light-driven TiO<sub>2</sub>-based heterojunctions for PPCP degradation: A critical review. *Water Res.* **2020**, *170*, 115356. [[CrossRef](#)] [[PubMed](#)]
132. Ong, W.J.; Tan, L.L.; Ng, Y.H.; Yong, S.T.; Chai, S.P. Graphitic Carbon Nitride (g-C<sub>3</sub>N<sub>4</sub>)-Based Photocatalysts for Artificial Photosynthesis and Environmental Remediation: Are We a Step Closer To Achieving Sustainability? *Chem. Rev.* **2016**, *116*, 7159–7329. [[CrossRef](#)] [[PubMed](#)]
133. Ahmed, S.N.; Haider, W. Heterogeneous photocatalysis and its potential applications in water and wastewater treatment: A review. *Nanotechnology* **2018**, *29*, 342001. [[CrossRef](#)] [[PubMed](#)]
134. McDaniel, H.; Heil, P.E.; Tsai, C.L.; Kim, K.; Shim, M. Integration of Type II Nanorod Heterostructures into Photovoltaics. *ACS Nano* **2011**, *5*, 7677–7683. [[CrossRef](#)]
135. Gou, J.F.; Ma, Q.L.; Deng, X.Y.; Cui, Y.Q.; Zhang, H.X.; Cheng, X.W.; Li, X.L.; Xie, M.Z.; Cheng, Q.F. Fabrication of Ag<sub>2</sub>O/TiO<sub>2</sub>-Zeolite composite and its enhanced solar light photocatalytic performance and mechanism for degradation of norfloxacin. *Chem. Eng. J.* **2017**, *308*, 818–826. [[CrossRef](#)]
136. Wang, W.; Fang, J.J.; Shao, S.F.; Lai, M.; Lu, C.H. Compact and uniform TiO<sub>2</sub>@g-C<sub>3</sub>N<sub>4</sub> core-shell quantum heterojunction for photocatalytic degradation of tetracycline antibiotics. *Appl. Catal. B* **2017**, *217*, 57–64. [[CrossRef](#)]
137. Hou, H.J.; Zhang, X.H.; Huang, D.K.; Ding, X.; Wang, S.Y.; Yang, X.L.; Li, S.Q.; Xiang, Y.G.; Chen, H. Conjugated microporous poly(benzothiadiazole)/TiO<sub>2</sub> heterojunction for visible-light-driven H<sub>2</sub> production and pollutant removal. *Appl. Catal. B* **2017**, *203*, 563–571. [[CrossRef](#)]
138. Ganguly, P.; Mathew, S.; Clarizia, L.; Kumar, R.S.; Akande, A.; Hinder, S.; Breen, A.; Pillai, S.C. Theoretical and experimental investigation of visible light responsive AgBiS<sub>2</sub>-TiO<sub>2</sub> heterojunctions for enhanced photocatalytic applications. *Appl. Catal. B* **2019**, *253*, 401–418. [[CrossRef](#)]
139. Liu, Z.; Tian, J.; Zeng, D.B.; Yu, C.L.; Huang, W.Y.; Yang, K.; Liu, X.Q.; Liu, H. Binary-phase TiO<sub>2</sub> modified Bi<sub>2</sub>MoO<sub>6</sub> crystal for effective removal of antibiotics under visible light illumination. *Mater. Res. Bull.* **2019**, *112*, 336–345. [[CrossRef](#)]
140. Yu, J.G.; Wang, S.H.; Low, J.X.; Xiao, W. Enhanced photocatalytic performance of direct Z-scheme g-C<sub>3</sub>N<sub>4</sub>-TiO<sub>2</sub> photocatalysts for the decomposition of formaldehyde in air. *Phys. Chem. Chem. Phys.* **2013**, *15*, 16883–16890. [[CrossRef](#)]
141. Mei, Q.F.; Zhang, F.Y.; Wang, N.; Lu, W.S.; Su, X.T.; Wang, W.; Wu, R.L. Photocatalysts: Z-Scheme Heterojunction Constructed with Titanium Dioxide. *Chin. J. Inorg. Chem.* **2019**, *35*, 1321–1339. [[CrossRef](#)]
142. Li, H.J.; Tu, W.G.; Zhou, Y.; Zou, Z.G. Z-Scheme Photocatalytic Systems for Promoting Photocatalytic Performance: Recent Progress and Future Challenges. *Adv. Sci.* **2016**, *3*, 1500389. [[CrossRef](#)] [[PubMed](#)]
143. Qi, K.Z.; Cheng, B.; Yu, J.G.; Ho, W.K. A review on TiO<sub>2</sub>-based Z-scheme photocatalysts. *Chin. J. Catal.* **2017**, *38*, 1936–1955. [[CrossRef](#)]
144. Low, J.X.; Jiang, C.; Cheng, B.; Wageh, S.; Al-Ghamdi, A.A.; Yu, J.G. A Review of Direct Z-Scheme Photocatalysts. *Small Methods* **2017**, *1*, 1700080. [[CrossRef](#)]
145. Meng, S.G.; Zhang, J.F.; Chen, S.F.; Zhang, S.J.; Huang, W.X. Perspective on construction of heterojunction photocatalysts and the complete utilization of photogenerated charge carriers. *Appl. Surf. Sci.* **2019**, *476*, 982–992. [[CrossRef](#)]
146. Wang, F.L.; Wu, Y.L.; Wang, Y.F.; Li, J.H.; Jin, X.Y.; Zhang, Q.X.; Li, R.B.; Yan, S.C.; Liu, H.J.; Feng, Y.P.; et al. Construction of novel Z-scheme nitrogen-doped carbon dots/{001} TiO<sub>2</sub> nanosheet photocatalysts for broad-spectrum-driven diclofenac degradation: Mechanism insight, products and effects of natural water matrices. *Chem. Eng. J.* **2019**, *356*, 857–868. [[CrossRef](#)]
147. Hao, J.G.; Zhang, S.F.; Ren, F.; Wang, Z.W.; Lei, J.F.; Wang, X.N.; Cheng, T.; Li, L.B. Synthesis of TiO<sub>2</sub>@g-C<sub>3</sub>N<sub>4</sub> core-shell nanorod arrays with Z-scheme enhanced photocatalytic activity under visible light. *J. Colloid Interface Sci.* **2017**, *508*, 419–425. [[CrossRef](#)]

148. Liao, W.J.; Murugananthan, M.; Zhang, Y.R. Synthesis of Z-scheme g-C<sub>3</sub>N<sub>4</sub>-Ti<sup>3+</sup>/TiO<sub>2</sub> material: An efficient visible light photoelectrocatalyst for degradation of phenol. *Phys. Chem. Chem. Phys.* **2015**, *17*, 8877–8884. [[CrossRef](#)]
149. Shayegan, Z.; Lee, C.S.; Haghghat, F. TiO<sub>2</sub> photocatalyst for removal of volatile organic compounds in gas phase—A review. *Chem. Eng. J.* **2018**, *334*, 2408–2439. [[CrossRef](#)]
150. Basavarajappa, P.S.; Patil, S.B.; Ganganagappa, N.; Reddy, K.R.; Raghu, A.V.; Reddy, C.V. Recent progress in metal-doped TiO<sub>2</sub>, non-metal doped/codoped TiO<sub>2</sub> and TiO<sub>2</sub> nanostructured hybrids for enhanced photocatalysis. *Int. J. Hydrog. Energy* **2020**, *45*, 7764–7778. [[CrossRef](#)]
151. Li, S.Y.; Yang, Y.L.; Su, Q.; Liu, X.Y.; Zhao, H.P.; Zhao, Z.X.; Li, J.; Jin, C. Synthesis and photocatalytic activity of transition metal and rare earth element co-doped TiO<sub>2</sub> nano particles. *Mater. Lett.* **2019**, *252*, 123–125. [[CrossRef](#)]
152. Oladipo, G.O.; Akinlabi, A.K.; Alayande, S.O.; Msagati, T.A.M.; Nyoni, H.H.; Ogunyinka, O.O. Synthesis, characterization, and photocatalytic activity of silver and zinc co-doped TiO<sub>2</sub> nanoparticle for photodegradation of methyl orange dye in aqueous solution. *Can. J. Chem.* **2019**, *97*, 642–650. [[CrossRef](#)]
153. Shahan, M.; Ahmed, A.M.; Shehata, N.; Betiha, M.A.; Rabie, A.M. Ni-doped and Ni/Cr co-doped TiO<sub>2</sub> nanotubes for enhancement of photocatalytic degradation of methylene blue. *J. Colloid Interface Sci.* **2019**, *555*, 31–41. [[CrossRef](#)]
154. Xia, H.Y.; Liu, G.Y.; Zhang, R.; Song, L.F.; Chen, H.X. The Photocatalytic Degradation of Vehicle Exhausts by an Fe/N/Co-TiO<sub>2</sub> Waterborne Coating under Visible Light. *Materials* **2019**, *12*, 3378. [[CrossRef](#)] [[PubMed](#)]
155. Sun, M.X.; Yao, Y.; Ding, W.; Anandan, S. N/Ti<sup>3+</sup> co-doping biphasic TiO<sub>2</sub>/Bi<sub>2</sub>WO<sub>6</sub> heterojunctions: Hydrothermal fabrication and sonophotocatalytic degradation of organic pollutants. *J. Alloys Compd.* **2020**, *820*, 153172. [[CrossRef](#)]
156. Bayan, E.M.; Lupeiko, T.G.; Pustovaya, L.E.; Volkova, M.G.; Butova, V.V.; Guda, A.A. Zn-F co-doped TiO<sub>2</sub> nanomaterials: Synthesis, structure and photocatalytic activity. *J. Alloys Compd.* **2020**, *822*, 153662. [[CrossRef](#)]
157. Zhao, L.; Xie, Y.Z.; Lin, Q.Y.; Zheng, R.Z.; Diao, Y. Preparation of C, N and P co-doped TiO<sub>2</sub> and its photocatalytic activity under visible light. *Funct. Mater. Lett.* **2019**, *12*, 1950045. [[CrossRef](#)]
158. Wang, H.X.; Zhu, L.N.; Guo, F.Q. Photoelectrocatalytic degradation of atrazine by boron-fluorine co-doped TiO<sub>2</sub> nanotube arrays. *Environ. Sci. Pollut. Res.* **2019**, *26*, 33847–33855. [[CrossRef](#)]
159. Yan, J.C.; Zhao, J.; Hao, L.; Hu, Y.F.; Liu, T.Y.; Guan, S.J.; Zhao, Q.; Zhu, Z.; Lu, Y. Low-temperature S-doping on N-doped TiO<sub>2</sub> films and remarkable enhancement on visible-light performance. *Mater. Res. Bull.* **2019**, *120*, 110594. [[CrossRef](#)]
160. Mohamed, R.M.; Bahnemann, D.W.; Basaleh, A.S.; Qadah, R.H. Photo-catalytic destruction of acetaldehyde using cobalt, copper co-doped titania dioxide nanoparticles beneath Visible light. *Appl. Nanosci.* **2020**, *10*, 931–939. [[CrossRef](#)]
161. Pham, T.D.; Lee, B.K. Selective removal of polar VOCs by novel photocatalytic activity of metals co-doped TiO<sub>2</sub>/PU under visible light. *Chem. Eng. J.* **2017**, *307*, 63–73. [[CrossRef](#)]
162. Isari, A.A.; Hayati, F.; Kakavandi, B.; Rostami, M.; Motevassel, M.; Dehghanifard, E. N, Cu co-doped TiO<sub>2</sub>@functionalized SWCNT photocatalyst coupled with ultrasound and visible-light: An effective sono-photocatalysis process for pharmaceutical wastewaters treatment. *Chem. Eng. J.* **2020**, *392*, 123685. [[CrossRef](#)]
163. Sharotri, N.; Sharma, D.; Sud, D. Experimental and theoretical investigations of Mn-N-co-doped TiO<sub>2</sub> photocatalyst for visible light induced degradation of organic pollutants. *J. Mater. Res. Technol.* **2019**, *8*, 3995–4009. [[CrossRef](#)]
164. Sirivallop, A.; Areerob, T.; Chiarakorn, S. Enhanced Visible Light Photocatalytic Activity of N and Ag Doped and Co-Doped TiO<sub>2</sub> Synthesized by Using an In-Situ Solvothermal Method for Gas Phase Ammonia Removal. *Catalysts* **2020**, *10*, 251. [[CrossRef](#)]
165. Chauhan, N.; Singh, V.; Kumar, S.; Sirohi, K. Preparation of palladium, silver, and nitrogen co-doped mesoporous titanium dioxide nanoparticles to investigate their photocatalytic action. *Mater. Res. Express* **2019**, *6*, 13. [[CrossRef](#)]
166. Osin, O.A.; Yu, T.Y.; Cai, X.M.; Jiang, Y.; Peng, G.T.; Cheng, X.M.; Li, R.B.; Qin, Y.; Lin, S.J. Photocatalytic Degradation of 4-Nitrophenol by C, N-TiO<sub>2</sub>: Degradation Efficiency vs. Embryonic Toxicity of the Resulting Compounds. *Front. Chem.* **2018**, *6*, 192. [[CrossRef](#)] [[PubMed](#)]

167. Zhao, Z.Y.; Feng, M.C.; Peng, Z.J.; Huang, H.W.; Guo, Z.H.; Li, Z.H. Molten-salt fabrication of (N,F)-codoped single-crystal-like titania with high exposure of (001) crystal facet for highly efficient degradation of methylene blue under visible light irradiation. *J. Mater. Res.* **2018**, *33*, 1411–1421. [[CrossRef](#)]
168. Wang, P.S.; Qi, C.X.; Wen, P.C.; Hao, L.Y.; Xu, X.; Agathopoulos, S. Synthesis of Si, N co-Doped Nano-Sized TiO<sub>2</sub> with High Thermal Stability and Photocatalytic Activity by Mechanochemical Method. *Nanomaterials* **2018**, *8*, 294. [[CrossRef](#)]
169. Zhang, J.Q.; Xing, Z.P.; Cui, J.Y.; Li, Z.Z.; Tan, S.Y.; Yin, J.W.; Zou, J.L.; Zhu, Q.; Zhou, W. C,N co-doped porous TiO<sub>2</sub> hollow sphere visible light photocatalysts for efficient removal of highly toxic phenolic pollutants. *Dalton Trans.* **2018**, *47*, 4877–4884. [[CrossRef](#)] [[PubMed](#)]
170. Singh, I.; Birajdar, B. Effective La-Na Co-Doped TiO<sub>2</sub> Nano-Particles for Dye Adsorption: Synthesis, Characterization and Study on Adsorption Kinetics. *Nanomaterials* **2019**, *9*, 400. [[CrossRef](#)]
171. Li, Y.F.; Xu, D.H.; Oh, J.I.; Shen, W.; Li, X.; Yu, Y. Mechanistic Study of Codoped Titania with Nonmetal and Metal Ions: A Case of C plus Mo Codoped TiO<sub>2</sub>. *ACS Catal.* **2012**, *2*, 391–398. [[CrossRef](#)]
172. Garg, A.; Singhanian, T.; Singh, A.; Sharma, S.; Rani, S.; Neogy, A.; Yadav, S.R.; Sangal, V.K.; Garg, N. Photocatalytic Degradation of Bisphenol-A using N, Co Codoped TiO<sub>2</sub> Catalyst under Solar Light. *Sci. Rep.* **2019**, *9*, 765. [[CrossRef](#)]
173. Wang, F.; Ma, Z.Z.; Ban, P.P.; Xu, X.H. C, N and S codoped rutile TiO<sub>2</sub> nanorods for enhanced visible-light photocatalytic activity. *Mater. Lett.* **2017**, *195*, 143–146. [[CrossRef](#)]
174. Wang, M.G.; Han, J.; Hu, Y.M.; Guo, R. Mesoporous C, N-codoped TiO<sub>2</sub> hybrid shells with enhanced visible light photocatalytic performance. *RSC Adv.* **2017**, *7*, 15513–15520. [[CrossRef](#)]
175. Modanlu, S.; Shafiekhani, A. Synthesis of pure and C/S/N co-doped Titania on Al mesh and their photocatalytic usage in Benzene degradation. *Sci. Rep.* **2019**, *9*, 16648. [[CrossRef](#)] [[PubMed](#)]
176. Zeng, X.L.; Sun, X.Z.; Yu, Y.S.; Wang, H.Y.; Wang, Y. Photocatalytic degradation of flumequine with B/N codoped TiO<sub>2</sub> catalyst: Kinetics, main active species, intermediates and pathways. *Chem. Eng. J.* **2019**, *378*, 122226. [[CrossRef](#)]
177. Humayun, M.; Raziq, F.; Khan, A.; Luo, W. Modification strategies of TiO<sub>2</sub> for potential applications in photocatalysis: A critical review. *Green Chem. Lett. Rev.* **2018**, *11*, 86–102. [[CrossRef](#)]
178. Zhu, K.; Neale, N.R.; Miedaner, A.; Frank, A.J. Enhanced charge-collection efficiencies and light scattering in dye-sensitized solar cells using oriented TiO<sub>2</sub> nanotubes arrays. *Nano Lett.* **2007**, *7*, 69–74. [[CrossRef](#)]
179. Zangeneh, H.; Zinatizadeh, A.A.L.; Habibi, M.; Akia, M.; Isa, M.H. Photocatalytic oxidation of organic dyes and pollutants in wastewater using different modified titanium dioxides: A comparative review. *J. Ind. Eng. Chem.* **2015**, *26*, 1–36. [[CrossRef](#)]
180. Toumazatou, A.; Arfanis, M.K.; Pantazopoulos, P.A.; Kontos, A.G.; Falaras, P.; Stefanou, N.; Likodimos, V. Slow-photon enhancement of dye sensitized TiO<sub>2</sub> photocatalysis. *Mater. Lett.* **2017**, *197*, 123–126. [[CrossRef](#)]
181. Diaz-Angulo, J.; Lara-Ramos, J.; Mueses, M.; Hernandez-Ramirez, A.; Li Puma, G.; Machuca-Martinez, F. Enhancement of the oxidative removal of diclofenac and of the TiO<sub>2</sub> rate of photon absorption in dye-sensitized solar pilot scale CPC photocatalytic reactors. *Chem. Eng. J.* **2020**, *381*, 122520. [[CrossRef](#)]
182. Park, H.; Park, Y.; Kim, W.; Choi, W. Surface modification of TiO<sub>2</sub> photocatalyst for environmental applications. *J. Photochem. Photobiol. C Photochem. Rev.* **2013**, *15*, 1–20. [[CrossRef](#)]
183. Choi, S.K.; Yang, H.S.; Kim, J.H.; Park, H. Organic dye-sensitized TiO<sub>2</sub> as a versatile photocatalyst for solar hydrogen and environmental remediation. *Appl. Catal. B* **2012**, *121*, 206–213. [[CrossRef](#)]
184. Dong, S.Y.; Feng, J.L.; Fan, M.H.; Pi, Y.Q.; Hu, L.M.; Han, X.; Liu, M.L.; Sun, J.Y.; Sun, J.H. Recent developments in heterogeneous photocatalytic water treatment using visible light-responsive photocatalysts: A review. *RSC Adv.* **2015**, *5*, 14610–14630. [[CrossRef](#)]
185. Diaz-Angulo, J.; Gomez-Bonilla, I.; Jimenez-Tohapanta, C.; Mueses, M.; Pinzon, M.; Machuca-Martinez, F. Visible-light activation of TiO<sub>2</sub> by dye-sensitization for degradation of pharmaceutical compounds. *Photochem. Photobiol. Sci.* **2019**, *18*, 897–904. [[CrossRef](#)] [[PubMed](#)]
186. Yun, E.T.; Yoo, H.Y.; Kim, W.; Kim, H.E.; Kang, G.; Lee, H.; Lee, S.; Park, T.; Lee, C.; Kim, J.H.; et al. Visible-light-induced activation of periodate that mimics dye-sensitization of TiO<sub>2</sub>: Simultaneous decolorization of dyes and production of oxidizing radicals. *Appl. Catal. B* **2017**, *203*, 475–484. [[CrossRef](#)]
187. Sengupta, D.; Das, P.; Mondal, B.; Mukherjee, K. Effects of doping, morphology and film-thickness of photo-anode materials for dye sensitized solar cell application—A review. *Renew. Sust. Energ. Rev.* **2016**, *60*, 356–376. [[CrossRef](#)]

188. Ahmad, I.; Kan, C.W. Visible-Light-Driven, Dye-Sensitized TiO<sub>2</sub> Photo-Catalyst for Self-Cleaning Cotton Fabrics. *Coatings* **2017**, *7*, 192. [[CrossRef](#)]
189. Murcia, J.J.; Avila-Martinez, E.G.; Rojas, H.; Cubillos, J.; Ivanova, S.; Penkova, A.; Laguna, O.H. Powder and Nanotubes Titania Modified by Dye Sensitization as Photocatalysts for the Organic Pollutants Elimination. *Nanomaterials* **2019**, *9*, 517. [[CrossRef](#)]
190. Guo, G.Q.; Guo, H.Y.; Wang, F.; France, L.J.; Yang, W.X.; Mei, Z.H.; Yu, Y.H. Dye-sensitized TiO<sub>2</sub>@SBA-15 composites: Preparation and their application in photocatalytic desulfurization. *Green Energy Environ.* **2020**, *5*, 114–120. [[CrossRef](#)]
191. Xu, T.Z.; Zhao, H.C.; Zheng, H.; Zhang, P.Y. Atomically Pt implanted nanoporous TiO<sub>2</sub> film for photocatalytic degradation of trace organic pollutants in water. *Chem. Eng. J.* **2020**, *385*, 123832. [[CrossRef](#)]
192. Lu, L.L.; Shan, R.; Shi, Y.Y.; Wang, S.X.; Yuan, H.R. A novel TiO<sub>2</sub>/biochar composite catalysts for photocatalytic degradation of methyl orange. *Chemosphere* **2019**, *222*, 391–398. [[CrossRef](#)]
193. Ismael, M. Enhanced photocatalytic hydrogen production and degradation of organic pollutants from Fe (III) doped TiO<sub>2</sub> nanoparticles. *J. Environ. Chem. Eng.* **2020**, *8*, 103676. [[CrossRef](#)]
194. Xu, J.J.; Chen, Y.F.; Dong, Z.Y.; Peng, Y.N.; Yue, S.T.; Huang, H. Strong effect of multi-electron oxygen reduction reaction on photocatalysis through the promotion of interfacial charge transfer. *Appl. Catal. B* **2019**, *252*, 41–46. [[CrossRef](#)]
195. Singh, K.; Harish, S.; Archana, J.; Navaneethan, M.; Shimomura, M.; Hayakawa, Y. Investigation of Gd-doped mesoporous TiO<sub>2</sub> spheres for environmental remediation and energy applications. *Appl. Surf. Sci.* **2019**, *489*, 883–892. [[CrossRef](#)]
196. Zhang, J.L.; Pang, Z.Y.; Sun, Q.; Chen, X.; Zhu, Y.A.; Li, M.J.; Wang, J.D.; Qiu, H.; Li, X.Q.; Li, Y.G.; et al. TiO<sub>2</sub> nanotube array modified with polypyrrole for efficient photoelectrocatalytic decolorization of methylene blue. *J. Alloys Compd.* **2020**, *820*, 153128. [[CrossRef](#)]
197. Singaram, B.; Jeyaram, J.; Rajendran, R.; Arumugam, P.; Varadharajan, K. Visible light photocatalytic activity of tungsten and fluorine codoped TiO<sub>2</sub> nanoparticle for an efficient dye degradation. *Ionics* **2019**, *25*, 773–784. [[CrossRef](#)]
198. Janbandhu, S.Y.; Joshi, A.; Munishwar, S.R.; Gedam, R.S. CdS/TiO<sub>2</sub> heterojunction in glass matrix: Synthesis, characterization, and application as an improved photocatalyst. *Appl. Surf. Sci.* **2019**, *497*, 143758. [[CrossRef](#)]
199. Liu, C.Q.; Li, X.; Wu, Y.T.; Zhang, L.Y.; Chang, X.J.; Yuan, X.X.; Wang, X.F. Fabrication of multilayer porous structured TiO<sub>2</sub>-ZrTiO<sub>4</sub>-SiO<sub>2</sub> heterostructure towards enhanced photo-degradation activities. *Ceram. Int.* **2020**, *46*, 476–486. [[CrossRef](#)]
200. Wang, R.; Shen, J.; Zhang, W.J.; Liu, Q.Q.; Zhang, M.Y.; Zulfiqar; Tang, H. Build-in electric field induced step-scheme TiO<sub>2</sub>/W<sub>18</sub>O<sub>49</sub> heterojunction for enhanced photocatalytic activity under visible-light irradiation. *Ceram. Int.* **2020**, *46*, 23–30. [[CrossRef](#)]
201. Thanh, T.L.T.; Thi, L.N.; Dinh, T.T.; Van, N.N. Enhanced Photocatalytic Degradation of Rhodamine B Using C/Fe Co-Doped Titanium Dioxide Coated on Activated Carbon. *J. Chem.* **2019**, *2019*, 2949316. [[CrossRef](#)]
202. Kumar, A.; Khan, M.; He, J.H.; Lo, I.M.C. Visible-light-driven magnetically recyclable terephthalic acid functionalized g-C<sub>3</sub>N<sub>4</sub>/TiO<sub>2</sub> heterojunction nanophotocatalyst for enhanced degradation of PPCPs. *Appl. Catal. B* **2020**, *270*, 118898. [[CrossRef](#)]
203. Chen, M.; Wang, H.H.; Chen, X.Y.; Wang, F.; Qin, X.X.; Zhang, C.B.; He, H. High-performance of Cu-TiO<sub>2</sub> for photocatalytic oxidation of formaldehyde under visible light and the mechanism study. *Chem. Eng. J.* **2020**, *390*, 124481. [[CrossRef](#)]
204. He, L.; Dong, Y.N.; Zheng, Y.N.; Jia, Q.M.; Shan, S.Y.; Zhang, Y.Q. A novel magnetic MIL-101(Fe)/TiO<sub>2</sub> composite for photo degradation of tetracycline under solar light. *J. Hazard. Mater.* **2019**, *361*, 85–94. [[CrossRef](#)] [[PubMed](#)]
205. Namshah, K.S.; Mohamed, R.M. WO<sub>3</sub>-TiO<sub>2</sub> nanocomposites for paracetamol degradation under visible light. *Appl. Nanosci.* **2018**, *8*, 2021–2030. [[CrossRef](#)]
206. Shi, Z.; Xu, P.F.; Shen, X.F.; Zhang, Y.; Luo, L.; Duoerkun, G.; Zhang, L.S. TiO<sub>2</sub>/MoS<sub>2</sub> heterojunctions-decorated carbon fibers with broad-spectrum response as weaveable photocatalyst/photoelectrode. *Mater. Res. Bull.* **2019**, *112*, 354–362. [[CrossRef](#)]
207. Djouadi, L.; Khalaf, H.; Boukhatem, H.; Boutoumi, H.; Kezzime, A.; Santaballa, J.A.; Canle, M. Degradation of aqueous ketoprofen by heterogeneous photocatalysis using Bi<sub>2</sub>S<sub>3</sub>/TiO<sub>2</sub>-Montmorillonite nanocomposites under simulated solar irradiation. *Appl. Clay Sci.* **2018**, *166*, 27–37. [[CrossRef](#)]

208. Leal, J.F.; Cruz, S.M.A.; Almeida, B.T.A.; Esteves, V.I.; Marques, P.; Santos, E.B.H. TiO<sub>2</sub>-rGO nanocomposite as an efficient catalyst to photodegrade formalin in aquaculture's waters, under solar light. *Environ. Sci. Water Res. Technol.* **2020**, *6*, 1018–1027. [[CrossRef](#)]
209. Morones-Esquivel, M.M.; Nunez-Nunez, C.M.; Gonzalez-Burciaga, L.A.; Hernandez-Mendoza, J.L.; Osorio-Revilla, G.I.; Proal-Najera, J.B. Kinetics and statistical approach for 2,5-dichlorophenol degradation in short reaction times by solar TiO<sub>2</sub>/glass photocatalysis. *Rev. Mex. Ing. Quim.* **2020**, *19*, 555–568. [[CrossRef](#)]
210. Borzyszkowska, A.F.; Pieczynska, A.; Ofiarska, A.; Lisowski, W.; Nikiforow, K.; Siedlecka, E.M. Photocatalytic degradation of 5-fluorouracil in an aqueous environment via Bi-B co-doped TiO<sub>2</sub> under artificial sunlight. *Int. J. Environ. Sci. Technol.* **2020**, *17*, 2163–2176. [[CrossRef](#)]
211. Tbessi, I.; Benito, M.; Molins, E.; Llorca, J.; Touati, A.; Sayadi, S.; Najjar, W. Effect of Ce and Mn co-doping on photocatalytic performance of sol-gel TiO<sub>2</sub>. *Solid State Sci.* **2019**, *88*, 20–28. [[CrossRef](#)]
212. Saqlain, S.; Cha, B.J.; Kim, S.Y.; Ahn, T.K.; Park, C.; Oh, J.M.; Jeong, E.C.; Seo, H.O.; Kim, Y.D. Visible light-responsive Fe-loaded TiO<sub>2</sub> photocatalysts for total oxidation of acetaldehyde: Fundamental studies towards large-scale production and applications. *Appl. Surf. Sci.* **2020**, *505*, 144160. [[CrossRef](#)]
213. Cherni, D.; Moussa, N.; Nsib, M.F.; Olivo, A.; Signoretto, M.; Prati, L.; Villa, A. Photocatalytic degradation of ethylbenzene in gas phase over N or NF doped TiO<sub>2</sub> catalysts. *J. Mater. Sci. Mater. Electron.* **2019**, *30*, 18919–18926. [[CrossRef](#)]
214. Jaleh, B.; Rouzbahani, M.G.; Abedi, K.; Azizian, S.; Ebrahimi, H.; Nasrollahzadeh, M.; Varma, R.S. Photocatalytic decomposition of VOCs by AC-TiO<sub>2</sub> and EG-TiO<sub>2</sub> nanocomposites. *Clean Technol. Environ. Policy* **2019**, *21*, 1259–1268. [[CrossRef](#)]
215. Kim, J.; Lee, B.K. Enhanced photocatalytic decomposition of VOCs by visible-driven photocatalyst combined Cu-TiO<sub>2</sub> and activated carbon fiber. *Process Saf. Environ. Prot.* **2018**, *119*, 164–171. [[CrossRef](#)]
216. Belet, A.; Wolfs, C.; Mahy, J.G.; Poelman, D.; Vreuls, C.; Gillard, N.; Lambert, S.D. Sol-gel Syntheses of Photocatalysts for the Removal of Pharmaceutical Products in Water. *Nanomaterials* **2019**, *9*, 126. [[CrossRef](#)]
217. Saif, M.; Aboul-Fotouh, S.M.K.; El-Molla, S.A.; Ibrahim, M.M.; Ismail, L.F.M. Evaluation of the photocatalytic activity of Ln(3+)-TiO<sub>2</sub> nanomaterial using fluorescence technique for real wastewater treatment. *Spectrochim. Acta Part A Mol. Biomol. Spectrosc.* **2014**, *128*, 153–162. [[CrossRef](#)]
218. Lima, K.V.; Emídio, E.S.; Pupo Nogueira, R.F.; do Vasconcelos, N.S.L.; Araújo, A.B. Application of a stable Ag/TiO<sub>2</sub> film in the simultaneous photodegradation of hormones. *J. Chem. Technol. Biotechnol.* **2020**, *8*. [[CrossRef](#)]
219. Peng, X.M.; Wang, M.; Hu, F.P.; Qiu, F.X.; Dai, H.L.; Cao, Z. Facile fabrication of hollow biochar carbon-doped TiO<sub>2</sub>/CuO composites for the photocatalytic degradation of ammonia nitrogen from aqueous solution. *J. Alloys Compd.* **2019**, *770*, 1055–1063. [[CrossRef](#)]
220. Li, S.M.; Tan, J.; Jiang, Z.J.; Wang, J.; Li, Z.Q. MOF-derived bimetallic Fe-Ni-P nanotubes with tunable compositions for dye-sensitized photocatalytic H<sub>2</sub> and O<sub>2</sub> production. *Chem. Eng. J.* **2020**, *384*, 123354. [[CrossRef](#)]
221. Saad, A.M.; Abukhadra, M.R.; Abdel-Kader Ahmed, S.; Elzanaty, A.M.; Mady, A.H.; Betiha, M.A.; Shim, J.-J.; Rabie, A.M. Photocatalytic degradation of malachite green dye using chitosan supported ZnO and Ce-ZnO nano-flowers under visible light. *J. Environ. Manag.* **2020**, *258*, 110043. [[CrossRef](#)] [[PubMed](#)]
222. Espino-Estevez, M.R.; Fernandez-Rodriguez, C.; Gonzalez-Diaz, O.M.; Arana, J.; Espinos, J.P.; Ortega-Mendez, J.A.; Dona-Rodriguez, J.M. Effect of TiO<sub>2</sub>-Pd and TiO<sub>2</sub>-Ag on the photocatalytic oxidation of diclofenac, isoproturon and phenol. *Chem. Eng. J.* **2016**, *298*, 82–95. [[CrossRef](#)]
223. Xu, H.F.; Li, G.; Liu, N.; Zhu, K.R.; Zhu, G.; Jin, S.W. Ag @ hierarchical TiO<sub>2</sub> core-shell nanostructures for enhanced photocatalysis. *Mater. Lett.* **2015**, *142*, 324–327. [[CrossRef](#)]
224. Ji, L.J.; Liu, X.; Xu, T.; Gong, M.D.; Zhou, S. Preparation and photocatalytic properties of carbon/carbon-doped TiO<sub>2</sub> double-layer hollow microspheres. *J. Sol-Gel Sci. Technol.* **2020**, *93*, 380–390. [[CrossRef](#)]
225. Fu, Z.T.; Zhang, S.; Fu, Z.X. Preparation of Multicycle GO/TiO<sub>2</sub> Composite Photocatalyst and Study on Degradation of Methylene Blue Synthetic Wastewater. *Appl. Sci. (Basel)* **2019**, *9*, 3282. [[CrossRef](#)]
226. He, X.; Wang, X.C.; Cheng, B.Z.; Cao, S.; Zhou, J.F. Application of Mn-doped Mesoporous TiO<sub>2</sub> in Tannery Wastewater Treatment. *J. Soc. Leather Technol. Chem.* **2019**, *103*, 318–322.
227. Bordes, M.C.; Vicent, M.; Moreno, R.; Garcia-Montano, J.; Serra, A.; Sanchez, E. Application of plasma-sprayed TiO<sub>2</sub> coatings for industrial (tannery) wastewater treatment. *Ceram Int.* **2015**, *41*, 14468–14474. [[CrossRef](#)]

228. Kim, K.H.; Kabir, E.; Jahan, S.A. Exposure to pesticides and the associated human health effects. *Sci. Total Environ.* **2017**, *575*, 525–535. [[CrossRef](#)]
229. Fiorenza, R.; Di Mauro, A.; Cantarella, M.; Iaria, C.; Scalisi, E.M.; Brundo, M.V.; Gulino, A.; Spitaleri, L.; Nicotra, G.; Dattilo, S.; et al. Preferential removal of pesticides from water by molecular imprinting on TiO<sub>2</sub> photocatalysts. *Chem. Eng. J.* **2020**, *379*, 122309. [[CrossRef](#)]
230. Abdennouri, M.; Baalala, M.; Galadi, A.; El Makhfouk, M.; Bensitel, M.; Nohair, K.; Sadiq, M.; Boussaoud, A.; Barka, N. Photocatalytic degradation of pesticides by titanium dioxide and titanium pillared purified clays. *Arab. J. Chem.* **2016**, *9*, S313–S318. [[CrossRef](#)]
231. Nasseh, N.; Taghavi, L.; Barikbin, B.; Nasser, M.A. Synthesis and characterizations of a novel FeNi<sub>3</sub>/SiO<sub>2</sub>/CuS magnetic nanocomposite for photocatalytic degradation of tetracycline in simulated wastewater. *J. Clean. Prod.* **2018**, *179*, 42–54. [[CrossRef](#)]
232. de Oliveira, C.P.M.; Viana, M.M.; Amaral, M.C.S. Coupling photocatalytic degradation using a green TiO<sub>2</sub> catalyst to membrane bioreactor for petroleum refinery wastewater reclamation. *Comp. Immunol. Microbiol. Infect. Dis.* **2019**, *68*, 101403. [[CrossRef](#)]
233. Ani, I.J.; Akpan, U.G.; Olutoye, M.A.; Hameed, B.H. Photocatalytic degradation of pollutants in petroleum refinery wastewater by TiO<sub>2</sub>- and ZnO-based photocatalysts: Recent development. *J. Clean. Prod.* **2018**, *205*, 930–954. [[CrossRef](#)]
234. Shivaraju, H.P.; Muzakkira, N.; Shahmoradi, B. Photocatalytic treatment of oil and grease spills in wastewater using coated N-doped TiO<sub>2</sub> polyscales under sunlight as an alternative driving energy. *Int. J. Environ. Sci. Technol.* **2016**, *13*, 2293–2302. [[CrossRef](#)]
235. Andronic, L.; Isac, L.; Miralles-Cuevas, S.; Visa, M.; Oller, I.; Duta, A.; Malato, S. Pilot-plant evaluation of TiO<sub>2</sub> and TiO<sub>2</sub>-based hybrid photocatalysts for solar treatment of polluted water. *J. Hazard. Mater.* **2016**, *320*, 469–478. [[CrossRef](#)]
236. Solis-Casados, D.A.; Escobar-Alarcon, L.; Gomez-Olivan, L.M.; Haro-Poniatowski, E.; Klimova, T. Photodegradation of pharmaceutical drugs using Sn-modified TiO<sub>2</sub> powders under visible light irradiation. *Fuel* **2017**, *198*, 3–10. [[CrossRef](#)]
237. Malakootian, M.; Olama, N.; Malakootian, M.; Nasiri, A. Photocatalytic degradation of metronidazole from aquatic solution by TiO<sub>2</sub>-doped Fe<sup>3+</sup> nano-photocatalyst. *Int. J. Environ. Sci. Technol.* **2019**, *16*, 4275–4284. [[CrossRef](#)]
238. Lacerda, J.A.S.; Macedo, A.M.; Teixeira, R.I.; Simoes, G.; Ribeiro, E.S.; Forero, J.S.B.; Correa, R.J. TiO<sub>2</sub> Decorated Sand Grains for Photodegradation of Pollutants: Methylene Blue and Ciprofloxacin Study. *J. Braz. Chem. Soc.* **2020**, *31*, 201–210. [[CrossRef](#)]
239. Hou, C.T.; Xie, J.Q.; Yang, H.L.; Chen, S.M.; Liu, H.L. Preparation of Cu<sub>2</sub>O@TiOF<sub>2</sub>/TiO<sub>2</sub> and its photocatalytic degradation of tetracycline hydrochloride wastewater. *RSC Adv.* **2019**, *9*, 37911–37918. [[CrossRef](#)]
240. Li, S.P.; Chang, L.B.; Peng, J.H.; Gao, J.Z.; Lu, J.B.; Zhang, F.C.; Zhu, G.Q.; Hojamberdiev, M. Bi-0 nanoparticle loaded on Bi<sup>3+</sup>-doped ZnWO<sub>4</sub> nanorods with oxygen vacancies for enhanced photocatalytic NO removal. *J. Alloys Compd.* **2020**, *818*, 152837. [[CrossRef](#)]
241. Rao, F.; Zhu, G.Q.; Hojamberdiev, M.; Zhang, W.B.; Li, S.P.; Gao, J.Z.; Zhang, F.C.; Huang, Y.H.; Huang, Y. Uniform Zn<sup>2+</sup>-Doped BiOI Microspheres Assembled by Ultrathin Nanosheets with Tunable Oxygen Vacancies for Super-Stable Removal of NO. *J. Phys. Chem. C* **2019**, *123*, 16268–16280. [[CrossRef](#)]
242. Zhang, G.X.; Sun, Z.M.; Duan, Y.W.; Ma, R.X.; Zheng, S.L. Synthesis of nano-TiO<sub>2</sub>/diatomite composite and its photocatalytic degradation of gaseous formaldehyde. *Appl. Surf. Sci.* **2017**, *412*, 105–112. [[CrossRef](#)]
243. Qin, Z.B.; Zhang, W.T.; Qian, G.P.; Wu, X.L.; Li, Y.J.M.R.I. The effects of different ways of adding nano-TiO<sub>2</sub> to concrete on the degradation performance of NO<sub>2</sub>. *Mater. Res. Innov.* **2015**, *19*, S10–S148. [[CrossRef](#)]
244. Zhang, J.H.; Hu, Y.; Qin, J.X.; Yang, Z.X.; Fu, M.L. TiO<sub>2</sub>-UiO-66-NH<sub>2</sub> nanocomposites as efficient photocatalysts for the oxidation of VOCs. *Chem. Eng. J.* **2020**, *385*, 123814. [[CrossRef](#)]
245. Wang, X.G.; Sun, M.H.; Muruganathan, M.; Zhang, Y.R.; Zhang, L.Z. Electrochemically self-doped WO<sub>3</sub>/TiO<sub>2</sub> nanotubes for photocatalytic degradation of volatile organic compounds. *Appl. Catal. B* **2020**, *260*, 118205. [[CrossRef](#)]
246. Lai, M.; Zhao, J.; Chen, Q.C.; Feng, S.J.; Bai, Y.J.; Li, Y.X.; Wang, C.Y. Photocatalytic toluene degradation over Bi-decorated TiO<sub>2</sub>: Promoted O<sub>2</sub> supply to catalyst's surface by metallic Bi. *Catal. Today* **2019**, *335*, 372–380. [[CrossRef](#)]

247. Rao, Z.P.; Xie, X.F.; Wang, X.; Mahmood, A.; Tong, S.R.; Ge, M.F.; Sun, J. Defect Chemistry of Er<sup>3+</sup>-Doped TiO<sub>2</sub> and Its Photocatalytic Activity for the Degradation of Flowing Gas-Phase VOCs. *J. Phys. Chem. C* **2019**, *123*, 12321–12334. [CrossRef]
248. Ali, N.; Bilal, M.; Khan, A.; Ali, F.; Iqbal, H.M.N. Effective exploitation of anionic, nonionic, and nanoparticle-stabilized surfactant foams for petroleum hydrocarbon contaminated soil remediation. *Sci. Total Environ.* **2020**, *704*, 135391. [CrossRef]
249. Peikam, E.N.; Jalali, M. Application of three nanoparticles (Al<sub>2</sub>O<sub>3</sub>, SiO<sub>2</sub> and TiO<sub>2</sub>) for metal-contaminated soil remediation (measuring and modeling). *Int. J. Environ. Sci. Technol.* **2019**, *16*, 7207–7220. [CrossRef]
250. Wang, L.; Li, X.; Tsang, D.C.W.; Jin, F.; Hou, D. Green remediation of Cd and Hg contaminated soil using humic acid modified montmorillonite: Immobilization performance under accelerated ageing conditions. *J. Hazard. Mater.* **2020**, *387*, 122005. [CrossRef]
251. Khalid, S.; Shahid, M.; Murtaza, B.; Bibi, I.; Natasha; Asif Naeem, M.; Niazi, N.K. A critical review of different factors governing the fate of pesticides in soil under biochar application. *Sci. Total Environ.* **2020**, *711*, 134645. [CrossRef]
252. Eker, G.; Hatipoglu, M. Effect of UV wavelength, temperature and photocatalyst on the removal of PAHs from industrial soil with photodegradation applications. *Environ. Technol.* **2019**, *40*, 3793–3803. [CrossRef]
253. Rachna; Rani, M.; Shanker, U. Degradation of tricyclic polyaromatic hydrocarbons in water, soil and river sediment with a novel TiO<sub>2</sub> based heterogeneous nanocomposite. *J. Environ. Manag.* **2019**, *248*, 109340. [CrossRef]
254. Zyoud, A.; Ateeq, M.; Helal, M.H.; Zyoud, S.H.; Hilal, H.S. Photocatalytic degradation of phenazopyridine contaminant in soil with direct solar light. *Environ. Technol.* **2019**, *40*, 2928–2939. [CrossRef]
255. Xu, Q.; Huang, Z.; Ji, S.T.; Zhou, J.; Shi, R.Z.; Shi, W.Y. Cu<sub>2</sub>O nanoparticles grafting onto PLA fibers via electron beam irradiation: Bifunctional composite fibers with enhanced photocatalytic of organic pollutants in aqueous and soil systems. *J. Radioanal. Nucl. Chem.* **2020**, *323*, 253–261. [CrossRef]
256. Theerakarunwong, C.D.; Phanichphant, S. Visible-Light-Induced Photocatalytic Degradation of PAH-Contaminated Soil and Their Pathways by Fe-Doped TiO<sub>2</sub> Nanocatalyst. *Water Air Soil Poll.* **2018**, *229*, 291. [CrossRef]
257. Kuang, X.; Shao, J.; Peng, L.; Song, H.; Wei, X.; Luo, S.; Gu, J.-D. Nano-TiO<sub>2</sub> enhances the adsorption of Cd(II) on biological soil crusts under mildly acidic conditions. *J. Contam. Hydrol.* **2020**, *229*, 103583. [CrossRef]
258. Yang, Y.; Javed, H.; Zhang, D.N.; Li, D.Y.; Kamath, R.; McVey, K.; Sra, K.; Alvarez, P.J.J. Merits and limitations of TiO<sub>2</sub>-based photocatalytic pretreatment of soils impacted by crude oil for expediting bioremediation. *Front. Chem. Sci. Eng.* **2017**, *11*, 387–394. [CrossRef]

